The Effect of Physiological Modulators on Resting-state fMRI Functional Connectivity.

by

Powell Pui Wai Chu

A thesis submitted in conformity with the requirements
for the degree of Master of Science
Department of Medical Biophysics
University of Toronto

The effect of physiological modulators on resting-state functional connectivity.

Powell Chu

Master of Science

Department of Medical Biophysics
University of Toronto

2016

Abstract

In this thesis, we focus on the following physiological modulators of the blood oxygenation level dependent (BOLD) signal — cerebral blood flow (CBF), venous-blood oxygenation, and cerebrovascular reactivity (CVR). We use simulations and experiments to examine the relationship between the physiological parameters with rs-fMRI functional connectivity measurements in three resting-state networks: default-mode network (DMN), sensori-motor network (SMN), and the visual network (VN). By using the general linear model, we demonstrate that physiological modulators significant impact functional connectivity measurements in these regions, both within subjects and between subjects. Moreover, we found that the physiological effects vary depending upon brain region and individual. The results confirm that it is important to account for the effect of physiological noise when examining resting-state fMRI functional connectivity, in the study of healthy brain function, but more importantly, in states of altered brain function.

Word count: 137/150

Contributions of Author

I am the first author of the manuscript on which chapters 2 is based. All work was carried out under the supervision of Dr. J. Jean Chen. My contributions are listed below.

1. Chu, P.P., Golestani, A.M., Kwinta, J.B., and Chen, J.J. *Physiological modulators of resting-state BOLD functional connectivity.* Submitted to NeuroImage 2016.

2. Chu, P. P., Golestani, A. M., Kwinta, J. B., Khatamian, Y. B., & Chen, J. J. *Physiological Modulators of Resting State MRI Functional Connectivity.* ISMRM 2015, Toronto. #2128.

Table of Contents

List of Tables

List of Figures

List of abbreviations and symbols

ASL	Arterial spin labeling
B_0 / B_1	Static / Excitation magnetic field
BOLD	Blood oxygen level-dependent
CBF	Cerebral blood flow
CBV	Cerebral blood volume
$CMRO_2$	Cerebral metabolic rate of oxygen
CO_2	Carbon dioxide
CSF	Cerebrospinal fluid
CVR	Cerebrovascular reactivity
dHb	Deoxyhemoglobin
oHb	Oxyhemoglobin
DMN	Default-mode network
EPI	Echo planar imaging
FC	Functional connectivity
fMRI	Functional magnetic resonance imaging
FOV	Field of view
FWHM	Full width at half maximum
HRF	Hemodynamic response function
MNI152	Montreal Neurological Institute standard brain atlas
NVC	Neurovascular coupling
O_2	Oxygen
OEF	Oxygen extraction fraction
pCASL	Pseudo-continuous arterial spin labeling
PET	Positron emission tomography
$PETCO_2$	Pressure of end-tidal carbon dioxide
REB	Research ethics board
ROI	Region of interest
rCBF	Regional cerebral blood flow
r_n	Correlation of noise components
r_s	Correlation of true signals
rs-fMRI	Resting-state functional magnetic resonance imaging
SMN	Sensori-motor network
SNR	Signal-to-noise ratio
T1	Longitudinal relaxation time
T2	Transverse relaxation time
TE / TR	Echo / Repetition time
TI	Inversion time
VN	Visual network
Y_a / Y_v	Arterial-/venous-blood oxygenation

Chapter 1

Background and motivation

1.1 Functional connectivity

Functional connectivity has been defined as the *temporal correlation between spatially remote neurophysiological events* (Friston, Frith et al. 1993). In recent neuroscience research, functional connectivity has been computed as the statistical association among brain signals from different brain regions. When different regions of the brain have high correlation according to their time-series data, they are said to be functionally connected. Conversely, when regions' temporal responses have low correlation value, they are said to be *not* functionally connected. Note that when two regions are functionally connected, they do not necessary have to be physically connected to each other.

Understanding functional connectivity allows us to know more about associations between different brain regions and this informs on the human brain function. Previously, using task-based functional magnetic resonance imaging (fMRI) we have been able to attribute specific functions to specific regions of the brain in a noninvasive manner. For instance, we understand that the motor cortex is responsible for the motor movement and occipital lobe is responsible for

visual processing (Purves, Augustine et al. 2001). In addition, through the concept of functional connectivity, we are now able to better understand more higher-order processing of the brain, such as the relationship between cognition and motor control (Hoffstaedter, Grefkes et al. 2014).

Functional connectivity was first examined through the relationship between electrophysiological measurements of different brain regions in response to electrical stimuli in *in vivo* animal studies (Finnerty and Jefferys 1993). In humans, early functional connectivity studies used electroencephalography (EEG) in task-based experiments (Koles and Flor-Henry 1987) by examining the differences in evoked potential during neuronal activation. Functional connectivity was also exemplified by subtraction techniques on images acquired from Positron Emission Tomography (PET) (Strother, Kanno et al. 1995, Becker, Mintun et al. 1996). Subsequently, the functional magnetic resonance imaging (fMRI) technique was used to examine functional connectivity based on the oxygenation level in different regions of the brain using blood oxygenation level dependent (BOLD) measurements (Biswal, Yetkin et al. 1995). By comparing the synchronicity of BOLD signals from different regions, functional connectivity maps were then formed to reveal functional networks. There have been studies that defined brain networks as either extrinsic or intrinsic, depicting the task-evoked and task-free networks, respectively (Mennes, Kelly et al. 2013). In particular, it was discovered that there are spontaneous fluctuations in the brain even during rest. Thus, scientists began to examine these brain responses, specifically functional connectivity in resting state.

1.1.1 Resting-state functional connectivity

The resting human brain accounts for only about 2% of the total body mass, but it consumes nearly 20% of the body's energy for neuronal response. The amount of energy that is consumed

during tasks relative to this basal metabolism is remarkably small (Raichle and Mintun 2006). Thus, it is important to look into the brain at rest in order to better understand its mechanism. In the resting state, studies have found that there exists low frequency fluctuations (<0.1 Hz) in the BOLD fMRI response, which is a widely used measurement that is used to evaluate the resting-state functional connectivity (Biswal, Hudetz et al. 1997, Yang, Long et al. 2007, Zang, He et al. 2007). Since cardiac and respiratory BOLD responses fluctuate at 0.8—1.2 Hz and 0.3 Hz respectively, the low frequency fluctuation is presumed to reflect neuronal activity (Raichle and Mintun 2006). Also, it has been shown that certain regions of the brain are more functionally connected than the others even in resting state (Smith, Fox et al. 2009), drawing attention to the study of how these fluctuations relate to each other (Fox, Snyder et al. 2005, Nasrallah, Yeow et al. 2015).

By examining functional connectivity of healthy individuals at rest, a number of resting-state networks have been identified, as illustrated in Figure 1.1 (Smith, Fox et al. 2009). Past literature has placed emphasis onto three widely studied networks, and they are the visual, default-mode, and sensorimotor networks. The first three networks in Figure 1.1 (Figure 1.1a—c) correspond to the medial, occipital pole, and the lateral visual areas. Together they formed the visual network, which is involved in visual processing. The default-mode network is depicted in Figure 1.1d, which consists of the precuneus, posterior cingulate cortex, inferior-lateral parietal and ventromedial frontal cortex. This network is interesting in that it is deactivated during tasks, and some studies have suggested its association with autobiographical memory, self, and theory of mind (Raichle, MacLeod et al. 2001, Greicius, Krasnow et al. 2003). The sensorimotor network is shown in Figure 1.1f, consisting of the supplementary motor area, sensorimotor cortex and

secondary somatosensory cortex, and it corresponds to planning and execution of voluntary movements and the sensory system.

For the purposes of this thesis, we will focus on three networks that have most robustly been observed, namely the visual, default-mode, and sensorimotor networks.

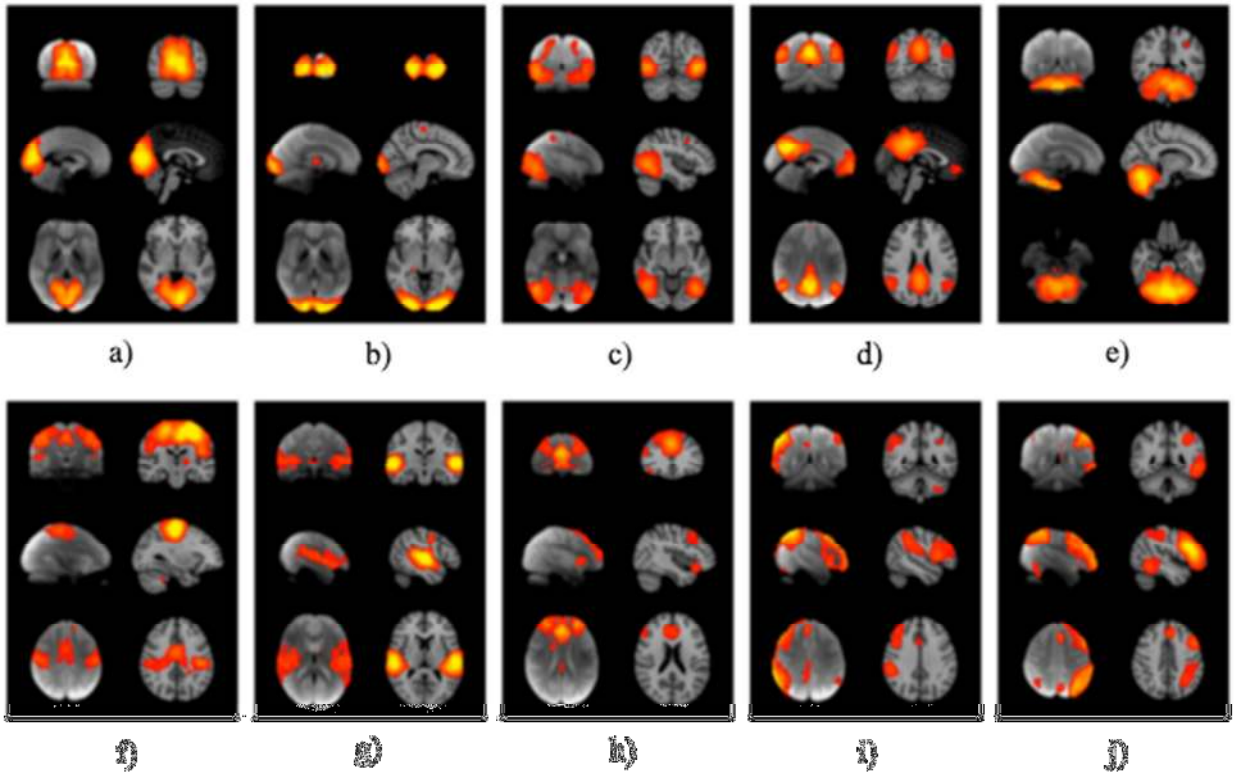

Figure 1.1: Resting-state functional networks, specifically the a) medial, b) occipital, and c) lateral visual areas, d) default-mode, e) cerebellar, f) sensorimotor, g) auditory, h) executive control, i) right frontoparietal, and j) left frontoparietal networks. Figure taken from (Smith, Fox et al. 2009).

One major advantage of resting-state fMRI over task-based fMRI is the absence of the need to perform any tasks. This means individuals from any background (age, ethnicity) and in any condition (conscious or unconscious, healthy or otherwise) can participate in the experiment.

This creates opportunities to examine functional connectivity of individuals in a clinical setting in hopes to understand more about the brain behavior in individuals with neurological diseases (Fox and Greicius 2010).

1.2 Magnetic resonance imaging (MRI)

The vast majority of resting-state functional connectivity studies have been performed using magnetic resonance imaging (MRI). MRI is a non-invasive imaging modality that is able to provide three-dimensional images within a human body. It is accomplished by examining the behavior of hydrogen protons in the presence of magnetic fields. Different tissue types have different magnetic spin properties, and this can be utilized to provide tissue-specific contrast with the help of magnetic fields, as described below.

In the absence of a strong static magnetic field, the hydrogen protons are oriented randomly. However, in the presence of a net magnetic field (B_0), the spins of the protons become polarized and are aligned either parallel or anti-parallel to the main axis of B_0, creating a net magnetization (M_0) in the longitudinal (B_0) direction. To obtain an MR signal, a radio-frequency (RF) excitation pulse (B_1) is applied at an angle from B_0, tipping away from the *longitudinal* magnetization (M_z) and creating a *transverse* magnetization component (M_{xy}) orthogonal to B_0. The spins of the protons are excited out of equilibrium.

When the RF transmitter is turned off, the transverse component of the magnetization decays while the longitudinal component recovers back to the net magnetization. This means that in this relaxation phase, M_{xy} decays to zero, while M_z approaches to M_0. T1 is defined as the spin-lattice relaxation time, namely the time constant at which 63% of the equilibrium longitudinal

magnetization is recovered, and T2 is defined as the spin-spin relaxation time, namely the time constant when 63% of the transverse magnetization is decayed. The above effects are summarized by the Bloch equation (Equation (1)), which expresses spin magnetization as a function of time with relaxation time constants T1 and T2:

$$\frac{d\boldsymbol{M}(t)}{dt} = \gamma\big(\boldsymbol{M}(t) \times \boldsymbol{B}(t)\big) - \frac{M_{xy}(t)}{T_2} - \frac{M_z(t) - M_0}{T_1} \quad (1)$$

where γ is the gyromagnetic ratio.

As the spins begin to dephase, transverse magnetization (M_{xy}) decreases. The spins can be rephrased by applying a 180° RF pulse using the so-called spin-echo (SE) technique. On the other hand, in gradient-echo (GRE) technique, the spin environment is additionally altered by gradient magnetic fields. First, a dephasing gradient lobe is applied right after the excitation pulse, causing rapid decay of the transverse magnetization. Then, by reversing the dephasing gradient, spins that were previously dephased begin to rephrase. The time for out-of-phase spins to be back into phase (creating an echo) is called the echo time (TE), and the time between two excitation pulses is defined as the repetition time (TR).

Echo planar imaging (EPI) is an imaging method that performs readout of M_{xy} by forming a train of echoes. This is accomplished by performing fast switching on the frequency- and phase-encoding gradients over the selected slice. EPI is the most common image-readout methods being used in fMRI.

In fMRI experiments, it is common to acquire T1-weighted images for anatomical reference. T1-weighted images are taken with short TR and short TE to minimize the effect of T2. In this case,

tissue with lower T1 value has greater signal intensity, since the longitudinal magnetization recovers faster after excitation. As an example, tissues with high fat content (white matter) have highest signal intensity, while tissues with high water content (CSF) appear dark. Conversely, T2-weighted images are taken with long TR and long TE to minimize the effect of T1. Tissue with smaller T2 value has lower signal intensity due to the faster decay in transverse magnetization.

In the presence of B_0 inhomogeneities, the transverse magnetization decays much faster than the decay given by T2. This effect is eliminated in a SE acquisition by the 180° pulse, but not in a GRE sequence. This rapid fast decay is defined as T2* decay, which occurs more quickly than T2 decay. This T2* effect is the basis of most BOLD fMRI studies, in which B_0 inhomogeneities can reflect deoxyhemoglobin content. By utilizing the paramagnetic property of deoxyhemoglobin, we can examine the behavior in each region of the brain through changes in the concentration of oxyhemoglobin and deoxyhemoglobin over time.

1.3 The BOLD signal

The BOLD fMRI technique has been the dominant MRI technique to evaluate brain activity. As mentioned earlier, the BOLD signal is influenced by the blood oxygenation status. Specifically, deoxyhemoglobin (dHb) are paramagnetic. The unpaired electron(s) create an electron magnetic dipole moment that causes field inhomogeneity, and thus reduces the signal intensity measured during the BOLD acquisition. On the other hand, oxyhemoglobin (oHb) are diamagnetic. Without unpaired electrons, they do not induce field inhomogeneities. Thus, the BOLD signal contrast comes from the MRI signal attenuation caused by deoxyhemoglobin, and that allows us to examine brain activity through blood-oxygenation levels.

When there is an increase in neural activity, more oxygen would be used, creating a more concentrated deoxyhemoglobin in capillaries and in veins. However, this triggers an increase in blood flow due to the neurovascular response, and that increases oxygenated blood being delivered to the brain and results in a reduction of concentration of deoxyhemoglobin. This in turn causes T2* to increase, and that increases the MR signal. This phenomenon is illustrated in Figure 1.2.

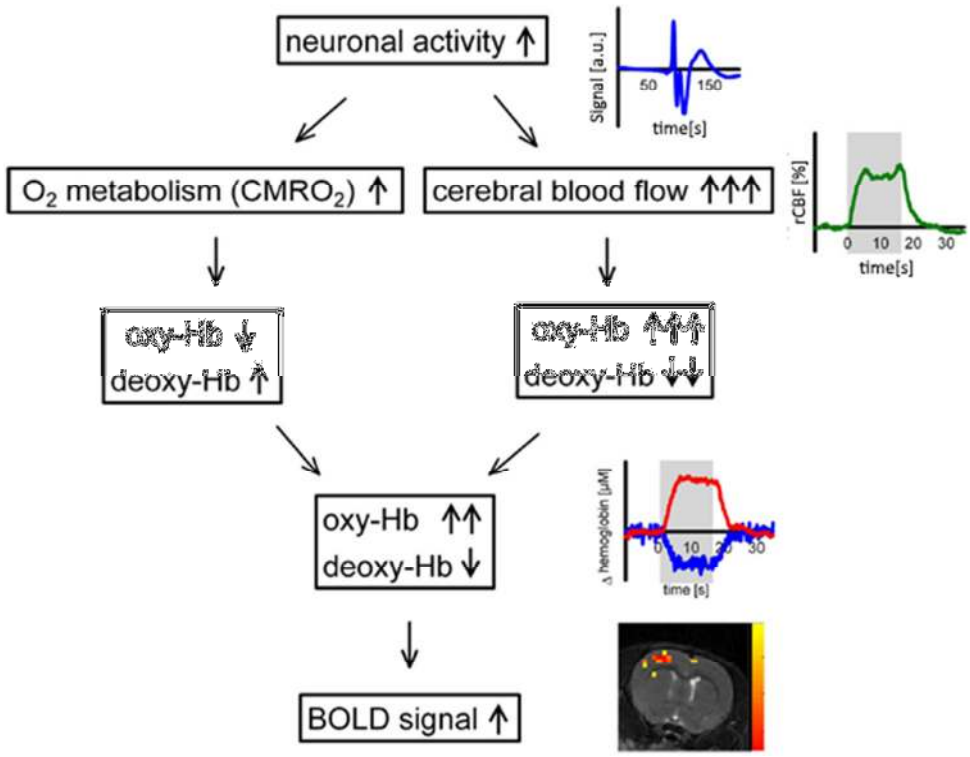

Figure 1.2: The neurovascular coupling effect. For instance, during increased neuronal activity. $CMRO_2$ increases, and thus dHb in vessels increase. However, due to neurovascular coupling, CBF increases more than $CMRO_2$, and thus oHb in vessels increase more than the increase in dHb. Thus, BOLD signal over all increases. The same applies to positive neuronal fluctuation in resting state. Figure taken from (Lindauer, Dirnagl et al. 2010).

1.4 Physiology

The brain requires a steady supply of glucose and oxygen to maintain metabolism. In the context of fMRI, the energy homeostasis of the brain can be characterized by 3 physiologic parameters: venous oxygenation level (Y_v), cerebral blood flow (CBF), and cerebral metabolic rate of oxygen ($CMRO_2$), as illustrated in Figure 1.3 (Lu, Xu et al. 2011). The flow rate of blood in the vasculature is denoted by CBF. Arterial vessels have an oxygenation level close to unity. When blood arrives at capillary beds, oxygen from a portion of oxyhemoglobin is extracted by brain tissue to support metabolism, expressed by $CMRO_2$, which directly reflects the neuronal firing rate (Maandag, Coman et al. 2007). The portion that remains in the blood will determine the venous oxygenation, Y_v, and is drained through veins. The venous blood eventually travels to the sinuses, particularly to the superior sagittal sinus and the inferior sagittal sinus. The superior and inferior sagittal sinuses are responsible to drain venous blood that comes from the cortical and subcortical regions of the brain, respectively. The venous blood then enters the internal jugular veins before returning to the heart.

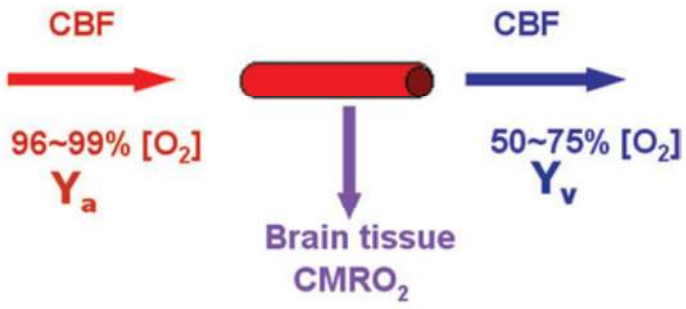

Figure 1.3: Energy homeostasis inside a capillary. Y_a denotes arterial oxygenation, and Y_v denotes venous oxygenation. Figure taken from (Lu, Xu et al. 2011).

An increase in neural response increases oxygen consumption, i.e. $CMRO_2$ (Hoge, Atkinson et al. 1999). As mentioned previously, the onset of an increase in neural response is followed by an often-disproportionate escalation in CBF. Since blood in arteries feeds highly oxygenated blood into capillaries, as CBF increases, oxygenation in capillaries increases as well. By the same token, rising CBF also increases the amount of blood travelling into the veins, and thus venous-blood oxygenation (Y_v) would also be affected. However, Y_v also varies with how much oxygen is being extracted in the capillaries, and thus it can vary even when CBF is constant. In addition, the CBF response depends on the extent of arterial and capillary elasticity, which is directly influenced by cerebrovascular reactivity (CVR), and it is to be discussed in a later section.

Thus, CBF and Y_v are linked to $CMRO_2$ due to the coupling effect between neural activity and the vascular response, as mentioned in (Lindauer, Dirnagl et al. 2010, Liu 2013). This relationship between neural fluctuations and vascular responses is defined as neurovascular coupling, and this phenomenon is also observed in (Kannurpatti, Motes et al. 2011), where the non-neural baseline physiological effects such as resting CBF (CBF_0), cerebral blood volume (CBV), CVR, and hematocrit levels also contribute to BOLD signal variability.

Neurovascular coupling effect was first observed in positron emission tomography (PET) studies. By using oxygen-15-labeled gases, it was discovered that a decrease in CBV and an increase in CBF/CBV ratio was associated with increased $CMRO_2$ (Leblanc, Tyler et al. 1987). In an fMRI study, Ogawa et al. first illustrated that BOLD-signal amplitude increased in a visual stimulation (Ogawa, Tank et al. 1992), suggesting that increases in CBF induced increases in the BOLD-signal amplitude during neuronal activity, and thus demonstrated the neurovascular coupling effect. In addition, dynamic metabolic changes were observed in resting state, and the

fluctuations in BOLD signal and CBF were synchronized with $CMRO_2$ fluctuations (Wu, Gu et al. 2009), suggesting neurovascular coupling effect remains imperative in resting state.

Even though the vascular response is affected by changes in neuronal response due to neurovascular coupling, the converse is not necessary true. This is further discussed later in this section.

1.5 BOLD-signal model

Past studies have tried to represent the BOLD signal with mathematical models to get a better understanding of the relationship between the vascular and neural responses. Instead of looking at BOLD signal intensity, which is arbitrary, the attention has been on modeling the *percent change* in BOLD signal (Liau and Liu 2009, Lu, Yezhuvath et al. 2010). The most well established BOLD-signal model is shown in Equation (2) (Davis, Kwong et al. 1998, Hoge, Atkinson et al. 1999, Liu, Hebrank et al. 2013):

$$\%\Delta BOLD = \frac{\Delta S}{S} = M\left[1 - \left(1 + \frac{\Delta CMRO_2}{CMRO_{2,0}}\right)^{\beta}\left(1 + \frac{\Delta CBF}{CBF_0}\right)^{\alpha-\beta}\right] \quad (2)$$

where

$$M = A * CBV_0 * TE * dHb_{conc} \quad (3)$$

$$CBV_0 = CBF_0^{\alpha} \quad (4)$$

In Equations (2)—(4), $CMRO_{2,0}$ is the baseline cerebral metabolic rate of oxygen [mol/100g/min], CBF_0 is the baseline (or resting) cerebral blood flow [ml/100g/min], CBV_0 is the

baseline blood volume [ml/100g], M is defined as the maximum possible BOLD signal change for a brain region, A is a multiplicative factor that depends on the magnetic strength, TE is the echo time [sec], and dHb_{conc} is the baseline concentration of deoxyhemoglobin (Hoge, Atkinson et al. 1999). dHb_{conc} can be further defined as

$$dHb_{conc} = K * Hct^{\beta} * (1 - Y_v)^{\beta} \quad (5)$$

where K is a scalar, Hct is the percentage of red blood cells per volume of blood [%], and Y_v is the baseline venous-blood oxygenation [%]. The exponential constant α represents the relationship between CBV and CBF (Grubb, Raichle et al. 1974), while β is dependent on field strength and MRI sequence parameters.

Equation (2) illustrates that the %ΔBOLD signal can be modeled as the interplay between neural (metabolic) and vascular responses, specifically the relationship between $CMRO_2$ and CBF, and this is referred to as neurovascular coupling. Some parameters of the model are relatively consistent across subjects, and their normal range of values is discussed in a later section. On the other hand, there are vascular parameters in the equation that vary both within-subject (different regions of the brain) and between subjects. These include CBV_0, CBF_0, and cerebrovascular reactivity, which can lead to subject-wise differences in BOLD amplitude variability (Kannurpatti, Motes et al. 2011).

1.5.1 Resting cerebral blood flow (CBF_0)

CBF_0 is the steady-state resting blood flow. This value can vary from region to region, depending on resting-state metabolic demands and blood-pressure autoregulation. That is, a given region can have higher blood flow if the size of the vessel is larger or if that region has

higher metabolic demands. Thus, CBF_0 can be affected by either neuronal activity or pure vascular response.

According to the BOLD-signal model in Equation (2), as CBF_0 increases, the %ΔBOLD signal decreases, assuming ΔCBF is positive. Thus, the %ΔBOLD signal also varies spatially within each subject due to variations in CBF_0, which has been suggested to be caused by the spatial differences in baseline $CMRO_2$ and neurovascular coupling. Thus, we can see that CBF_0 plays an important role in BOLD signal variability across subjects, and it is interesting to see the effect of this variability has on fMRI-based functional connectivity values.

It is important to distinguish CBF_0 from changes in CBF (ΔCBF). The percent change in regional CBF (rCBF) showed a negative correlation with baseline rCBF during a visual stimulation, but the absolute increase in rCBF was not correlated with baseline rCBF (Kastrup, Li et al. 1999). This suggests that it is necessary to pay close attention to the value of CBF_0 when comparing %ΔCBF values. Different individuals with different CBF_0 have been associated with significantly different amplitudes and shapes in their BOLD responses (Cohen, Ugurbil et al. 2002). Elevated CBF_0 has been shown to cause strong attenuation in BOLD response (Stefanovic, Warnking et al. 2006), and inter-subject differences in BOLD activation amplitude are correlated with resting CBF (Liau and Liu 2009). This suggests that steady-state vascular differences of CBF_0 are responsible for BOLD signal variation.

1.5.2 Global venous-blood oxygenation (Y_v)

As mentioned earlier, venous blood contains deoxyhemoglobin (dHb), which is paramagnetic and causes MRI field inhomogeneities, and that reduces the BOLD fMRI signal intensity. When

there is an increase in blood flow, the concentration of dHb is reduced, leading to less attenuation in the BOLD signal (Hoge, Atkinson et al. 1999).

Recall from the previous section, CBF_0 can significantly affect BOLD-signal amplitude. Since CBF_0 also affects Y_v, it would be interesting to see the underlying effect of Y_v on the BOLD response and on functional connectivity. Also, from Equation (2), we can see a direct relationship between the %ΔBOLD with Y_v. If we assume that Y_v and CBF_0 are decoupled, then as global Y_v increases, the %ΔBOLD signal decreases, assuming a positive ΔCBF. This means the deoxyhemoglobin content in veins is reduced, causing less BOLD signal attenuation, and thus the %ΔBOLD signal decreases.

CBF_0 can be affected by neuronal activity or vascular response. Since Y_v is directly influenced by CBF_0, Y_v is also affected depending if it is neuronal or vascular responses (Lu, Zhao et al. 2008). With an increase in metabolic activity, Y_v decreases. %ΔCBF also increases due to neurovascular coupling, and hence %ΔBOLD increases. On the other hand, for pure vascular changes, with an increase in CBF_0, Y_v increases, and the increase in both CBF_0 and Y_v causes %ΔBOLD to decrease. Thus, it is important to understand the cause of Y_v variability in order to interpret %ΔBOLD signal thoroughly.

While Y_v cannot be mapped on a voxel-wise basis using MRI, Y_v is intrinsically linked to oxygen extraction fraction (OEF), which is defined as the fraction of oxygen that is extracted from the blood vessels by the tissue (Liu, Hebrank et al. 2013).

$$OEF = \frac{(Y_a - Y_v)}{Y_a}\ [\%] \tag{6}$$

where Y_a represents the percentage of arterial-blood oxygenation. Since arterial blood often contains abundant supply of oxyhemoglobin, Y_a is usually assumed to be 100%. Thus, OEF is directly related to Y_v as:

$$OEF = 1 - Y_v\ [\%] \tag{7}$$

Past literature has examined OEF using positron emission tomography (PET), and it has shown that its value is very similar across different regions of the brain (Hyder, Herman et al. 2016). This illustrates that whole brain OEF, or equivalently Y_v, can potentially be represented by a global-averaged value.

1.5.3 Cerebrovascular reactivity (CVR)

CVR is a metric that evaluates the capacity for vasodilation and vasoconstriction of blood vessels. Blood vessels with high CVR have the ability to vary blood flow *relative to its baseline value*. Thus, CVR is defined as the %ΔCBF. From the BOLD-signal model in Equation (2), as CVR increases, the %ΔCBF increases, and thus the %ΔBOLD signal increases, and their relationship is linear and becomes non-linear above a certain value of %ΔCBF (Hoge, Atkinson et al. 1999). Thus, for most common applications, CVR can be approximated through the BOLD response associated with the CBF response.

Past studies have used either breath-hold task or CO_2 inhalation (hypercapnia) to examine CVR (Tancredi and Hoge 2013). In a visual stimulation experiment, it has been discovered that the

BOLD response increased linearly with the pressure in end-tidal CO_2 level ($PETCO_2$) (Cohen, Ugurbil et al. 2002), and the slope of it has later been termed as CVR. Thus,

$$CVR = \frac{\%\Delta BOLD}{\Delta PETCO_2} \tag{8}$$

CO_2 challenges have been widely used in the literature to examine CVR (Kety and Schmidt 1948), based on the premise that mild and transient changes in intravascular CO_2 level do not affect cerebral metabolic activity. This assumption has been verified in the literature (Chen and Pike 2010, Jain, Langham et al. 2011). Thus, CO_2 inhalation can be used to induce pure vascular changes (Nasrallah, Yeow et al. 2015). With CO_2 inhalation, arterial pressure of CO_2 rises, which induces an increase in the size of the blood vessels in the brain. This increase in %ΔCBF allows CVR to be measured.

There is a direct relationship between CVR and neurovascular coupling. As CVR decreases, the contribution of CBF due to motor stimulation becomes less (Salinet, Robinson et al. 2015). This means that the effect neural activity on CBF decreases, affecting the neurovascular coupling ratio. Such a scenario can be observed in aging, whereby a decrease in CVR was found with advancing age, along with decreasing CBF_0 and increased $CMRO_2$ (Lu, Xu et al. 2011). This illustrates that CVR modulates neurovascular coupling effect along with aging (D'esposito, Zarahn et al. 1999).

According to the BOLD-signal model, %ΔCBF directly influences the value of the %ΔBOLD signal. This hemodynamic response increases the oxygen transportation to the site of neuronal activation (Khalili-Mahani, van Osch et al. 2012). During neural fluctuations, CBF fluctuates

more than $CMRO_2$, and that leads to changes in OEF and the deoxyhemoglobin concentration, causing a fluctuation in BOLD signal intensity (Buxton, Uludag et al. 2004). In the context of CVR, as CVR decreases, %ΔCBF decreases (Lu, Xu et al. 2011), and vice versa. This variation in hemodynamic response is not necessarily dependent on metabolic activity, and may lead to variations in the neurovascular coupling effect and hence in the BOLD signal (in both amplitude and frequency). This phenomenon can be observed in Figure 1.4. The effects of delay, temporal broadening, and attenuation of hemodynamic response cause attenuations of the BOLD response (Liu 2013). Such changes can significantly alter the correlation (and by extension, functional connectivity) between two BOLD responses.

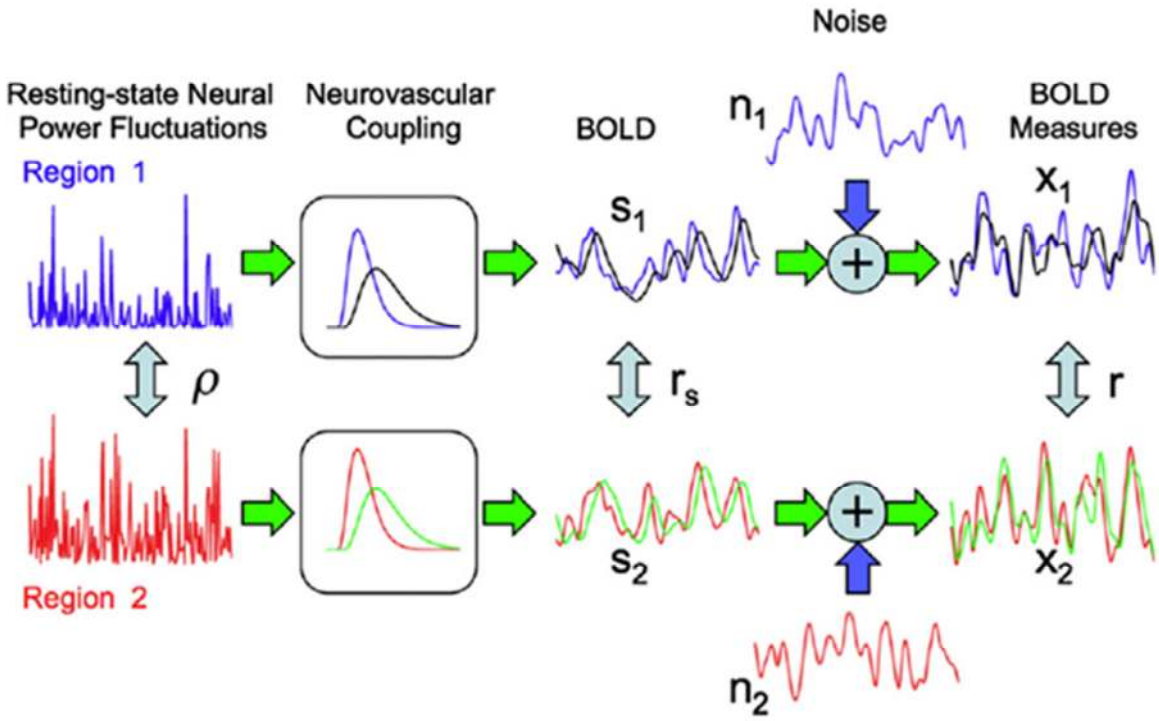

Figure 1.4: Illustration in the meaning of measured BOLD signal. The convolution of neuronal activity with the hemodynamic response function yields the BOLD signal. The measured BOLD signal consists of the true BOLD signal and its noise component. With a temporal boardening and attenuation in hemodynamic response function, the BOLD signal becomes attenuated (black and green). Figure taken from (Liu 2013).

A recent study has shown resting-state functional connectivity to be significantly correlated with CVR in the motor and executive control network (Golestani, Kwinta et al. 2016), and it will be interesting to look at the relative impact of CVR to functional connectivity in the presence of other physiological variations (i.e. CBF_0, Y_v).

1.6 Global physiological effects

In the previous section, we have illustrated that according to the BOLD-signal model, the %ΔBOLD signal depends on three physiological parameters: resting cerebral blood flow (CBF_0), global venous-blood oxygenation (Y_v), and cerebrovascular reactivity (CVR). The main reason we have focused on these parameters is because of their effect on the resting-state BOLD signal irrespective to local neural activity. For instance, resting-state functional connectivity has also been shown to be reduced in the default-mode network in normal aging (Damoiseaux, Beckmann et al. 2008), but the origins of this reduction may not be purely neuronal.

Y_v typically ranges between 50 and 75 % in healthy adults (Nagdyman, Fleck et al. 2005, Lu, Zhao et al. 2008), meaning deoxyhemoglobin content varies between 25 and 50%. This variability creates a large BOLD-signal variability across subjects. In addition, different individuals also have different vasodilatory capabilities and resting-state blood pressure, and thus leading to differences in CVR. CVR can also be diminished in individuals with vascular risk (Reinhard, Schwarzer et al. 2014) and aging (Lu, Xu et al. 2011). Moreover, CBF_0 has been reported to decrease in normal aging (Chen, Rosas et al. 2011). Moreover, age-associated increase in $CMRO_2$ has also been reported (Xu, Rowley et al. 2010, Lu, Xu et al. 2011, Peng, Dumas et al. 2014). OEF has also been found to be increased significantly with age (Peng, Dumas et al. 2014). This means that higher demand in oxygen is met by extracting more oxygen,

rather than an increase in CBF. The combination of higher demand and lower supply results in a reduction of Y_v with age. This illustrates that there is a change in neurovascular coupling with age, which can be translated into BOLD-signal variations that are not directly related to $CMRO_2$ variations.

Physiological parameters are also affected by physical condition and pharmacological manipulations. Substances such as alcohol and morphine change the relationship of BOLD fluctuations with $CMRO_2$, specifically the neurovascular coupling effect (Khalili-Mahani, van Osch et al. 2012). Caffeine also alters neurovascular coupling, but it does not alter CVR during hypercapnia (Chen and Parrish 2009). Different levels of CO_2 and O_2 in arterial blood also changes the BOLD signal activation amplitude (Nasrallah, Yeow et al. 2015). Specifically, increase in either CO_2 or O_2 causes an increase in venous-blood oxygenation, and thereby decreases the BOLD-signal amplitude.

In summary, there is a large variability in the physiological parameters, either across subjects or in different conditions. This variability affects the %ΔBOLD signal. However, this variability may be independent from neurometabolic activity. As shown in the past literature, changes to the vasculature induced by CO_2 inhalation do not vary the metabolic activity (Nasrallah, Yeow et al. 2015). Moreover, the sparse literature on physiological modulations of fMRI has focused on tasked-based experiment (Liu, Hebrank et al. 2013), while similar studies on resting-state functional connectivity measurements have not been conducted. This knowledge motivates the research to examine the effect of these physiological modulators and to account for these effects when examining neuronal fluctuations using resting-state fMRI.

1.7 Signal-to-noise ratio (SNR) with functional connectivity

As shown in Figure 1.4, the measured BOLD signal reflects a combination of true BOLD signal and noise contributions. When we are looking at the correlation (or connectivity) between two measured BOLD signals, we are really looking at the combination of correlations between the signal components s_1 and s_2, *and* correlations between the noise components n_1 and n_2. This is summarized by the following equation (Liu 2013),

$$r = r_s \left(\frac{SNR + \left({}^{r_n}/_{r_s} \right)}{SNR + 1} \right) \tag{9}$$

where r_s is the correlation between the true signals, r_n is the correlation between the noise components, SNR is the signal-to-noise ratio, assuming the SNR for one source is the same as the SNR for the other. We can find the graphical representation of the Equation (9) in Figure 1.5. When the correlation of the signal components is greater than the noise components, the correlation between the measured BOLD signals increases and saturates as SNR increases, and vice versa when the correlation of the noise components is greater than the signal components. The temporal SNR (tSNR) in resting state has been discovered to be around 2 to 4 for 32-Ch coil (Triantafyllou, Polimeni et al. 2011). With such a low SNR value, the effects of r_n and r_s become significant. Recall that CBF_0, Y_v, and CVR can vary substantially in both within and across subjects, resulting in variability in the BOLD signal. The combination of both the physiological modulators and the noise components play an important role in determining the functional connectivity between two *measured* %ΔBOLD signals.

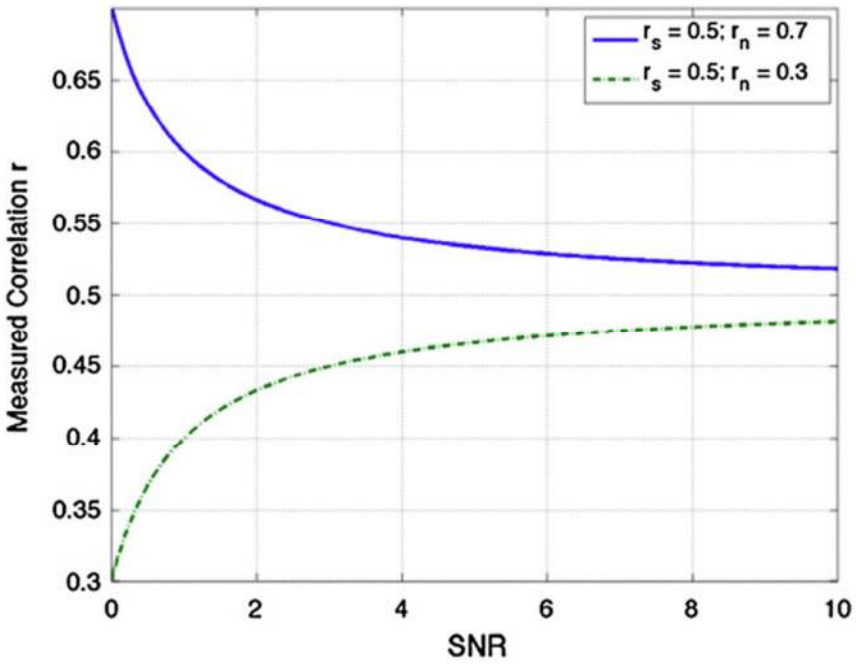

Figure 1.5: Graphic representation of Equation (9). Figure taken from (Liu 2013).

In BOLD fMRI, the noise component can be represented by the following equation:

$$\sigma_t = \sqrt{{\sigma_0}^2 + {\sigma_p}^2} \tag{10}$$

where $\sigma_t, \sigma_0, \sigma_p$ is the standard deviation of total noise, thermal noise, and physiological noise respectively (Triantafyllou, Polimeni et al. 2011). Physiological noise can be represented by the respiratory and cardiac fluctuations, and their frequencies are 0.1 to 0.5 Hz and 0.6 to 1.2 Hz respectively. There also exists low-frequency fluctuations from the cardiac and respiratory fluctuations, and their frequencies are around 0.01 Hz and 0.03 Hz respectively (Shmueli, van Gelderen et al. 2007, Birn, Smith et al. 2008). The effect of thermal noise should be the same to any regions of the brain, but the physiological noise varies within and across subjects. It has been shown that low frequency fluctuations dominate the effect of respiratory and cardiac fluctuations

in a task-based experiment (Cordes, Haughton et al. 2001). However, due to the lack of a stimulus, we are only observing the neurovascular fluctuations in resting state. Thus, the effects of respiratory and cardiac fluctuations in resting-state analysis are likely to be greater than those in task-based experiment, and that motivates our focus in examining the physiological noise components.

1.8 Existing literature on resting-state functional connectivity

The effect of CBF on %ΔBOLD and functional connectivity in resting state has previously been examined in the literature. Liang et al. have discovered that regional CBF_0 is significantly correlated with functional connectivity strength in the default-mode network and the executive control network in resting state (Liang, Zou et al. 2013). In another study, Li et al. have shown that functional connectivity and CBF are highly correlated in some regions of the default-mode network (Li, Zhu et al. 2012). While this is similar to the focus of this research, the authors did not address the effect of other physiological modulators, specifically Y_v and CVR, nor did they examine specifically into the functional connectivity of other resting-state networks. Moreover, they did not address which of the three parameters holds larger influence over rs-fcMRI measures, especially given the strong interplay between functional connectivity and SNR.

1.9 Thesis Objectives

The sensitivity of resting-state fMRI functional connectivity (rs-fcMRI) is hampered by physiological effects that introduce additional variability. This variability may contribute critical limitations that impede the clinical translation of resting state fcMRI.

Thus far, there has been no study that examines the associations of the multiple physiological modulators in resting-state BOLD functional connectivity measurements, and that is the primary goal of this research, with a focus on resting-state functional connectivity in the default-mode network (DMN), sensorimotor network (MN), and the visual network (VN). **We hypothesize that (1) CBF_0, CVR and Y_v influence resting-state fcMRI measurements in significant but distinct manners; (2) the influences of these variables also depend on the temporal SNR of the fMRI data.**

The findings of this project will help us better understand neurovascular interactions in BOLD signal fluctuations and the difference between the signal variation in normal population and those with disease (Fox and Greicius 2010).

Chapter 2

The effect of physiological modulators on resting-state fMRI functional connectivity

Note: This chapter has been submitted as a manuscript for publication in NeuroImage.

2.1 Introduction

The BOLD fMRI signal can be modeled as the interplay between neural (metabolic) and vascular responses, specifically the interrelationship of the cerebral metabolic rate of oxygen ($CMRO_2$) and cerebral blood flow (CBF). Moreover, there are vascular parameters in the well-known BOLD-signal model (Hoge, Atkinson et al. 1999, Wu, Gu et al. 2009) that vary both within subject (across different regions of the brain) and between subjects. These include resting cerebral blood flow/volume (CBF_0/CBV_0), venous-blood oxygenation (Y_v) and cerebrovascular reactivity (CVR), which can lead to subject-wise differences in resting-state BOLD amplitude variability (Kannurpatti, Motes et al. 2011). These parameters have previously been shown to relate to biases in task-related BOLD response amplitudes (Liu, Hebrank et al. 2013). However, their impact on resting-state fMRI (rs-fMRI) and related functional connectivity (rs-fcMRI) measurements has not been studied. Such physiological influences could contribute to additional

inter-subject variability in rs-fcMRI metrics, potentially undermining the sensitivity of such measures to quantify true inter-subject differences in brain function. In this work, we will focus on the same physiological modulators previously examined by Liu *et al.* in a task-based paradigm, i.e. CBF_0, Y_v and CVR.

CBF_0 can vary from region to region, depending on resting-state metabolic demands and blood-pressure autoregulation. That is, a given region can have higher blood flow if the size of the vessel is larger or if that region has higher metabolic demands. Thus, CBF_0 can be affected by either neuronal activity or pure vascular response. CBF_0 was previously found to negatively correlate with task-related BOLD response amplitude at a sub-significant level (Liu, Hebrank et al. 2013).

Y_v is also affected depending if it is neuronal or vascular responses (Lu, Zhao et al. 2008). With an increase in metabolic activity, Y_v decreases. On the other hand, the CBF response presumably follows the neural activity patterns due to neurovascular coupling, and with an increase in CBF_0, Y_v increases, and the increase in both CBF_0 and Y_v causes the BOLD signal to decrease. Thus, it is important to understand the cause of Y_v variability in order to interpret the BOLD signal thoroughly. Once again, Liu *et al.* found Y_v to be negatively associated with task-related BOLD amplitude (Liu, Hebrank et al. 2013).

CVR is a metric that evaluates the capacity for vasodilation and vasoconstriction of blood vessels. Blood vessels with higher CVR have the ability to vary their blood flow to a greater extent *relative to its baseline value*. Thus, the influence of CVR on the BOLD signal can be defined through the ratio of changes in CBF and in $CMRO_2$. For most common applications, CVR can be approximated through the BOLD response associated with the CBF response. As

expected, CVR was found to be positively associated with task-related BOLD-response amplitude (Liu, Hebrank et al. 2013).

If we assume that the resting-state BOLD signal, to some degree, follows the steady-state BOLD-signal model, then we can expect that the rs-fMRI signal amplitude to be modulated by the same physiological modulators. Moreover, an additional complication regarding functional connectivity is that the dependence of rs-fcMRI measurements on temporal signal-to-noise ratio (SNR) has been shown to be nonlinear (Liu 2013). In this work, we address these issues theoretically and empirically. We adopt a simulation-driven approach, in which we predict the effect of each physiological variable on rs-fcMRI measurements. The simulation results are then used to inform our experimental results. Our results indicate that physiological modulation of rs-fcMRI measurements varies across brain regions and depends on the predicted temporal SNR of the rs-fMRI signal.

2.2 Materials and methods

2.2.1 Simulations

We model the BOLD signal according to the BOLD biophysical model (Davis, Kwong et al. 1998, Hoge, Atkinson et al. 1999). A similar approach was previously taken by Wu *et al.* (Wu, Gu et al. 2009).

$$\frac{\Delta BOLD(t)}{BOLD_0} = M\left[1-\left(1+\frac{\Delta CMRO_2(t)}{CMRO_{2,0}}\right)^{\beta}\left(1+\frac{\Delta CBF(t)}{CBF_0}\right)^{\alpha-\beta}\right] \tag{11}$$

where $CMRO_2$ is cerebral metabolic rate of oxygen, CBF is cerebral blood flow, α, β and M are constants which depend on physiological and acquisition parameters, and the subscript '0'

denotes baseline. Specifically, M is defined as the maximum possible BOLD signal change for a brain region. Furthermore,

$$M = A * CBF_0^{\alpha} * TE * dHb_{conc} \quad (12)$$

where A is a multiplicative factor that depends on the magnetic strength, TE is the echo time, and dHb_{conc} is the baseline concentration of deoxyhemoglobin (Hoge, Atkinson et al. 1999). dHb_{conc} can be further defined as

$$dHb_{conc} = K * Hct^{\beta} * (1 - Y_v)^{\beta} \quad (13)$$

where K is a scalar, Hct is the percentage of red blood cells per volume of blood, and Y_v is the percentage of baseline venous-blood oxygenation.

While we recognize that this model is an oversimplification and is intended for steady-state BOLD signal, and that it has not been explicitly validated for resting-state BOLD signal, this approach nonetheless offers an accessible biophysical framework to guide our understanding of the physiological nature of the resting BOLD signal. Within this framework, our simulation was implemented through the following steps.

1. We simulated resting-state $CMRO_2$ time courses being representative of neuronal activity fluctuations. The time courses assumed a noise-free sinusoidal pattern, with a frequency of 50 Hz. This simplistic representation is based on the previously demonstrated associations between the BOLD signal and gamma oscillations (Balduzzi, Riedner et al. 2008). Note that this assumption does not affect conclusions drawn from the simulation.
2. Functional connectivity between two neural sources (r_s) is modulated by shifting their

respective signals with respect to each other; in this case, we are simulating an r_s of approximately 0.5 as the true functional connectivity. Note that this value is meant to allow sufficient range to simulate varying relationships between signal- and noise-induced correlations, and the choice of this value does not alter the simulation outcomes.

3. The amplitude of the neuronal fluctuations ($\Delta CMRO_2$) is set to 5 % above and below the mean resting $CMRO_2$; this is intended to be much lower than values typically observed during tasks (between 15% and 30%) (Tagliazucchi, von Wegner et al. 2012).
4. Resting-state CBF (CBF_0) is assumed to be 52.8 ml/100 g/min in human grey matter based on Ito *et al.* (Ito, Kanno et al. 2003). The resting-state CBF fluctuations are assumed to be coupled to those of $CMRO_2$, but scaled by a factor that corresponds to the neurovascular-coupling ratio. The typical range of this ratio during tasks is between 2 and 4 (Chiarelli, Bulte et al. 2007), whereas in resting state, this range may be extended. Our choice of CBF_0 and the neurovascular-coupling ratio (CBF:$CMRO_2$ ratio) depended on the variable of interest, and is detailed later in this section.
5. The value of M depends on Y_v, as shown in Equation (13).
6. The product of all terms of the right side of Equation (11) is then convolved with the canonical hemodynamic response function (HRF) derived based on functional activation (Glover 1999). This was taken to be the resting-state BOLD signal.
7. The assumed values of other variables are listed in Table 2.1Table 2.1: Simulation parameters..

Table 2.1: Simulation parameters.

Parameter	Simulated Value	Source
K	1	Arbitrary value for constant
A	1	Arbitrary value for constant
α	0.2	(Chen and Pike 2009, Chen and Pike 2010)
β	1.3	(Uludağ, Müller-Bierl et al. 2009)
Hct	0.4	Men: 40 to 54%; Women: 36 to 48%, (Billett 1990)
TE	0.030 s	According to our rs-fMRI acquisition protocol
$CMRO_{2,0}$	164.1 umol/100g/min	(Lu, Xu et al. 2011)
CBF_0	52.8 ml/100g/min	(Ito, Kanno et al. 2003)
CVR factor ($\Delta CBF:\Delta CMRO_2$)	3	Midrange of values in (Chiarelli, Bulte et al. 2007)
Y_v	0.6	(Liu, Huang et al. 2014)

CBF_0 and Y_v are potentially linked through the Kety and Schmidt equation (Kety and Schmidt 1948). That is

$$CMRO_2 = CBF \times (1 - Y_v) \tag{14}$$

However, in the interest of isolating the influence of each physiological variable on rs-fcMRI measurements, we assumed for simulation purposes that CBF_0, Y_v and CVR are independent of one another.

2.2.1.1 Resting Cerebral Blood Flow (CBF_0)

When assessing the effect of CBF_0 (through the value of *M*, as indicated in Equation (12)), we fixated the $\%\Delta CBF:\%\Delta CMRO_2$ ratio to 3, based on the average of past-reported values , and varied CBF_0 between 10 and 100 ml/100 g/min. Thus, Equations (11) and (12) reduce to

$$\frac{\Delta BOLD(i,t)}{BOLD_0} = M(i)\left[1 - \left(1 + \frac{\Delta CMRO_2(t)}{164.1\ [umol/100g/min]}\right)^{1.3}\left(1 + \frac{\Delta CBF(t)}{CBF_0(i)}\right)^{-1.1}\right] \tag{15}$$

And

$$M(i) = CBF_0(i)^{0.2} * 0.03[s] * 0.4^{1.3} * (1 - 0.6)^{1.3} \quad (16)$$

where the index *i* moves through all simulated CBF_0 values.

2.2.1.2 Venous Oxygenation (Y_v)

Venous oxygenation can vary based on resting levels of oxidative metabolism. Given that the flow-metabolism coupling (neurovascular-coupling ratio) varies across individuals, we can assume the rate of oxidative metabolism varies across individuals irrespective of their CBF_0 values. In this case, $\Delta CBF:\Delta CMRO_2$ ratio is again assumed to be 3, and CBF_0 is taken as 52.8 ml/100g/min. Equations (11) and (12) reduce to

$$\frac{\Delta BOLD(i,t)}{BOLD_0} = M(i)\left[1 - \left(1 + \frac{\Delta CMRO_2(t)}{164.1[umol/100g/min]}\right)^{1.3}\left(1 + \frac{\Delta CBF(t)}{52.8[ml/100g/min]}\right)^{-1.1}\right] \quad (17)$$

And

$$M(x) = (52.8[ml/100g/min])^{0.2} * 0.03[s] * 0.4^{1.3} * (1 - Y_v(i))^{1.3} \quad (18)$$

where the index *i* moves through all simulated Y_v values.

2.2.1.3 Cerebrovascular Reactivity (CVR)

In terms of Equation (11), CVR is an important factor in determining the extent of CBF response to $CMRO_2$ changes (Maggio, Salinet et al. 2014). One can also appreciate that CVR, which does

not have direct neuronal effects, can substantially modulate the BOLD signal and thus introduce ambiguity into the measurement interpretations, particularly in the presence of vascular pathology. This effect has in fact been demonstrated in healthy adults (Golestani, Kwinta et al. 2016). To simulate the effect of CVR, we modulated the value of the CBF:$CMRO_2$ coupling ratio between 1.5 and 5, in keeping with past findings (Hoge 2012); we assumed that $Y_v = 0.6$ and $CBF_0 = 52.8$ ml/100g/min. In this case, Equations (11) and (12) reduce to

$$\frac{\Delta BOLD(i,t)}{BOLD_0} = M(i)\left[1 - \left(1 + \frac{\Delta CMRO_2(t)}{164.1[umol/100g/min]}\right)^{1.3}\left(1 + \frac{\Delta CBF(t)}{52.8[ml/100g/min]}\right)^{-1.1}\right] \quad (19)$$

And

$$M(i) = (52.8[ml/100g/min])^{0.2} * 0.03[s] * 0.4^{1.3} * (1 - Yv(i))^{1.3} \quad (20)$$

where the index *i* moves through all simulated Y_v values.

2.2.1.4 Noise Model

The SNR characteristics of rs-fMRI acquisition has previously been investigated in (Triantafyllou, Polimeni et al. 2011). In this paper, temporal SNR (tSNR) is related to image SNR (SNR_0) through the following system of equations.

$$tSNR^2\left(1 + \lambda^2 {SNR_0}^2\right) = SNR_0 \quad (21)$$

$$\frac{\sigma_p}{\sigma_0} = \sqrt{\left(\frac{SNR_0}{tSNR}\right)^2 - 1} \quad (22)$$

where σ_p is the standard deviation of the physiological noise and σ_0 is the standard deviation of thermal noise. As we used 32-channel acquisition with a voxel size of 4 mm x 4 mm x 3 mm (close to our own acquisition choice), $\frac{\sigma_p}{\sigma_0} = 3.93$. Also, $\lambda_{32ch} = 0.0081$. Based on these values, SNR_0 was estimated to be approximately 16.2, and tSNR was approximately 4. Thus, we are simulating a range of tSNRs between 2 and 6, to accommodate less-than-ideal acquisition conditions. The simulated signal-noise combination is then computed based on this range of tSNR values,

$$\sigma_s = \frac{||s||_2}{\sqrt{L_s}} \tag{23}$$

$$SNR = \frac{\sigma_s}{\sigma_n} \tag{24}$$

where $||s||_2$ is the Euclidean norm of signal and L_s is the length of the signal. The magnitude of the noise, characterized by σ_n, is computed as the Euclidean of thermal noise (σ_0) and physiological noise (σ_p).

$$\sigma_n = \sqrt{{\sigma_0}^2 + {\sigma_p}^2} \tag{25}$$

Thermal noise is uniformly distributed across all sampled frequencies, whereas physiological noise is the sum of the following simulated sinusoidal waveforms:

- Time-locked respiratory noise at 0.3 Hz;
- Time-locked cardiac at noise 1.0 Hz;
- Low frequency cardiac and respiratory variability, at 0.01 Hz and 0.03 Hz, respectively (Shmueli, van Gelderen et al. 2007, Birn, Smith et al. 2008).

As it is difficult to ascertain the weighting of these different noise types, for simulation purposes, when considering the additive effect of different noise sources, we assumed identical weighting

for all noise sources. However, unlike thermal noise, physiological noise may be spatially coherent in certain regions, mimicking true functional connectivity patterns. Thus, we simulated three sets of noise scenarios:

- Thermal noise only: assuming physiological noise to be negligible, more likely when SNR_0 is low;
- Functional connectivity estimates dominated by true signal: this is a scenario discussed in (Liu 2013), in which the correlation between the physiological noise components (r_n) of the two neural sources, is set to be approximately 0.21, well below the true-signal driven correlation of $r_s = 0.54$.

Functional connectivity estimates dominated by physiological noise: this is contrary to the above scenario, in that the measured correlation coefficient is in fact dominated by correlation between noise components; that is, $r_n = 0.91$ while r_s remains at 0.54.

2.2.2 MRI Acquisition

We performed MRI experiments on 15 healthy participants, (6 men, 9 women), aged from 18 to 43 years (mean = 25.7 years, SD = 6.6). Participants were recruited through the Baycrest Participants Database, consisting of individuals from the Baycrest and local communities. The study was approved by the research ethics board (REB) of Baycrest, and the experiments were performed with the understanding and written consent of each participant, according to REB guidelines.

Images were acquired using a Siemens TIM Trio 3 T System (Siemens, Erlangen, Germany). The scans employed 32-channel phased- array head coil reception and body-coil transmission. A 3D T_1-weighted anatomical scan was acquired using MPRAGE, with resolution 1 × 1 × 1 mm,

repetition time (TR) = 2400 ms, inversion time (TI) =1000 ms, echo time (TE) = 2.43 ms, flip angle = 8°, field of view = 256 × 256 mm (sagittal), matrix size = 256 × 256, 192 slices (ascending order), bandwidth = 180 Hz/pixel, and GRAPPA acceleration factor = 2.

For functional connectivity measurements, resting-state BOLD scans were acquired using slice-accelerated scanning for more accurate noise removal, using the simultaneous multi-slice GE-EPI BOLD technique (Setsompop, Gagoski et al. 2012): TR/TE = 380/30 ms, flip angle = 40°, 15 slices of 6.25 mm thickness, 64x64 matrix, 3.44x3.44x6.25 mm voxels, axial oblique orientation, a multi-band factor of 3 with an in-plane phase shift factor of 2.

For assessing CBF_0 and BOLD-based CVR, we acquired resting-state CBF and BOLD data simultaneously using a dual-echo pCASL sequence (Dai et al., 2008). Detailed scanning protocols are as follows: TR = 3500 ms, TE_{CBF}/TE_{BOLD} = 10/25 ms, field of view = 220 × 220 mm, matrix size = 64 × 64, 20 slices (ascending interleaved order), voxel size = 3.44 × 3.44 × 6.0 mm^3, the number of time frames = 100, bandwidth = 2520 Hz/pixel, and GRAPPA acceleration factor = 2. The labeling duration was 1500 ms, and the post-labeling delay was 1000 ms with a mean G_Z of 1 mT/m was selected to achieve transit time insensitivity.

During the CVR scans, $PETCO_2$ was sinusoidally modulated (Blockley, Driver et al. 2011) during the dual-echo pCASL scans with a period of 120 s; 3 periods of sinusoidal $PETCO_2$ variations were induced with a baseline-to-peak amplitude of ±4 mmHg, following a 1-minute baseline. This sinusoidal manipulation was applied at the 3 vascular-tension levels described earlier.

Venous blood T_2 was obtained in vivo for each subject in the superior sagittal sinus using a magnetization-prepared segmented EPI sequence (Stefanovic and Pike 2004, Chen and Pike 2009), which was previously used successfully to determine mean Y_v in the internal jugular veins (Chen and Pike 2010). We used a Carr-Purcell-Meiboom-Gill (CPMG) refocusing interval of 6 ms.

2.2.3 Data Analysis

2.2.3.1 Preprocessing

Functional images, including the tag and control images in the pCASL data, and T_1-weighted anatomical images were separately preprocessed using SPM8 (Wellcome Trust Centre for Neuroimaging, London, UK, (Friston, Holmes et al. 1995)) and FSL (FMRIB Centre, Oxford). The first four time frames were discarded to ensure a steady-state MR signal. Preprocessing for functional images included retrospective head motion correction, slice-timing correction using sinc interpolation, spatial transformation into a Montreal Neurological Institute (MNI152) space, and spatial smoothing with a 6-mm full-width at half-maximum (FWHM) Gaussian kernel.

2.2.3.2 Functional connectivity

We band-pass filtered the rs-fMRI data to the 0.008 – 0.09 Hz range. Note that due to our high sampling rate (TR = 0.38 s), we were able to directly filter out the fundamental cardiac and respiratory frequencies. We recognize that higher-order harmonics may remain, albeit their amplitudes should be much lower than that of the fundamental frequency peak.

Anatomical images were co-registered with their corresponding realigned functional data and segmented into gray and white matter tissue probability maps using unified segmentation

(Ashburner and Friston 2005). Exploiting this anatomical information, we assume that the physiological noise contribution arising from low-frequency cardiac pulsation and respiration is globally distributed, and that the white matter and cerebrospinal fluid (CSF) could serve as noise regions-of-interest (ROI). The first 6 principal components derived from the signal in the noise ROIs were then removed by projection onto the orthogonal complement of the range space of the noise regressors. In addition, we regressed out frame-by-frame head motion (3 displacement and 3 rotational parameters as well as their first-order temporal derivatives).

As mentioned earlier, we focused on the motor, visual and default-mode networks. For each resting-state network, we carried out seed-based approach to obtain the connectivity maps (Yeo, Krienen et al. 2011, Whitfield-Gabrieli and Nieto-Castanon 2012, Tak, Polimeni et al. 2015). The diameter of each seed is 8 mm, and their coordinates are listed in Table 2.2. Each seed is used to bring out each functional connectivity map, and the maps are averaged to compute the final map for each resting-state network.

Table 2.2: Seed-coordinates for each resting-state network in MNI space.

Network	Seed Region	Abbreviation	X	Y	Z
Default-mode	Posterior cingulate cortex	PCC	-6	-52	40
	Medial prefrontal cortex	MPFC	-1	49	-5
	Lateral parietal cortex (left)	LLP	-46	-70	36
	Lateral parietal cortex (right)	RLP	46	-70	36
Sensorimotor	Primary motor cortex (left)	MNL	-42	-26	62
	Primary motor cortex (right)	MNR	42	-26	62
Visual	Primary visual cortex (left)	V1L	-12	-100	-8
	Primary visual cortex (right)	V1R	14	-100	-8

2.2.3.3 Basal cerebral blood flow

To assess the contribution of baseline CBF to the resting-state BOLD–CBF relationship, CBF maps were generated from the pCASL data using the ASL Data Processing Toolbox (ASLtbx) (Wang, Aguirre et al. 2008).

2.2.3.4 Venous oxygenation

From these T_2 measurements, venous oxygenation (Y_v) was estimated using the calibration relationship (T_2 dependence on blood oxygenation and CPMG refocusing interval obtained by Chen and Pike (2009) based on in vitro whole human blood relaxometry (Chen and Pike 2009) and the weak field-inhomogeneity diffusion model (Jensen and Chandra 2000).

2.2.3.5 Cerebrovascular reactivity

For the CVR calculation, the BOLD signal was calculated by averaging consecutive tag and control images from the second echo of the pCASL data. First, the CO_2-response delay in BOLD time course was accounted for at each voxel. This delay was estimated from the phase difference between the BOLD or CBF time courses and that of $PETCO_2$, enabling the alignment of the fMRI and $PETCO_2$ time series for maximal correlation. For this alignment, both $PETCO_2$ and fMRI data were upsampled to a common higher frequency, such that delays that are shorter than TR could be measured. Following the alignment, the $PETCO_2$ was interpolated to the pCASL TR and detrended at half the total duration of the respiratory paradigm. Outlier removal was performed based on Cook's distance from the initial linear model fit and the points with the Cook's distance greater than 4/N is discarded, where N is the number of time points (Bollen and Jackman 1990). Subsequently, a linear model is fitted to the BOLD (dependent variable) and

$PETCO_2$ (independent variable) values and CVR is defined as the slope of the linear model. The spatially specific CVR was thresholded at 0 to minimize biases introduced by noise, as we do not expect negative CVR values in the grey matter of healthy young adults. Additionally, we excluded data associated with spiking in $PETCO_2$ time course. We computed the regional mean and standard deviation of the CVR estimates across each resting-state network.

2.2.3.6 Statistical analyses

2.2.3.6.1 Group voxel-wise analysis

To facilitate group-analysis, the anatomical-registered CBF_0, CVR and functional-connectivity maps were sampled into MNI152 space using FMRIB Software Library (FSL) (Analysis Group, FMRIB, Oxford, UK) (Smith et al., 2004). These sets of maps were then concatenated, and voxel-wise general-linear model (GLM) analysis was then performed using FreeSurfer (http://surfer.nmr.mgh. harvard.edu). We assessed the effect of each physiological modulators (CBF_0, Y_v and CVR) on functional connectivity maps in each of the three networks (default-mode, sensorimotor, and visual networks), and the GLM analysis was carried out on each physiological modulator independently from the effects of the other modulators. The results were sampled onto the FreeSurfer spherical surface for visualization, at a depth of 50% into the cortical ribbon. This approach was designed to minimize the inclusion of voxels contaminated with white matter or CSF.

2.2.3.6.2 Region-of-interest (ROI) analysis

In order to assess the degree of Y_v modulation that is due to CBF_0, as suggested by Equation (14)**,** within each network region, we computed the mean CBF_0 and regressed it out of the global Y_v measurement to obtain the residual Y_v. In each ROI, we further modeled the effect of CBF_0

on fcMRI measures, and regressed that out of the Y_v measurements, resulting in residual fcMRI values. A ROI-based method was chosen as we only have a single Y_v measurement per subject. We subsequently assessed the linear relationship between residual Y_v and fcMRI measurements.

2.2.3.6.3 Within-subject voxel-wise analysis

To provide insight on the group results, we also performed within-subject voxel-wise general-linear model analyses. That is, in each subject's native space, we extracted voxel-wise functional connectivity values from each network of each subject, and regressed these against the voxel-wise CBF_0 or CVR values from the same voxels. Within each ROI, we ensured that there were no skews in the distributions of the functional connectivity, CBF_0 and CVR values. Moreover, prior to the GLM, we performed two additional steps to maximize the accuracy of our statistics: (1) To alleviate the degree of large-sample biases in the p-values (Lin, Lucas Jr. et al. 2012), we stratified each the voxel-wise data vectors into 50 bins of equal sample size, since the larger the number of samples, the higher the possibility of Type 1 errors, and the higher the chance of incorrectly rejecting the null hypothesis (Salkind 2010). (2) As functional connectivity values are likely to exhibit spatial autocorrelation within each set of voxels, we first performed the Durbin-Watson test on the data to be fitted, to establish the degree of spatial autocorrelation, then used the Cochrane-Orcutt method to correct the autocorrelation, and finally repeating the Durbin-Watson test to ensure that the autocorrelation has sufficiently been removed.

2.3 Results

2.3.1 Simulations

The simulations indicate the CVR and Y_v have the strongest impact on fcMRI outcome, followed by CBF_0. The specific findings are discussed below.

2.3.1.1 Resting cerebral blood flow (CBF_0)

There is a positive linear relationship between functional connectivity and CBF_0 when r_s is greater than r_n (Figure 2.1a), and a negative linear relationship when r_s is less than r_n (Figure 2.1b). In both cases, the relationship tends to disappear as SNR increases. Without the effect of the physiological noise (i.e. when only thermal noise is present), there is effectively no correlation between CBF_0 and functional connectivity.

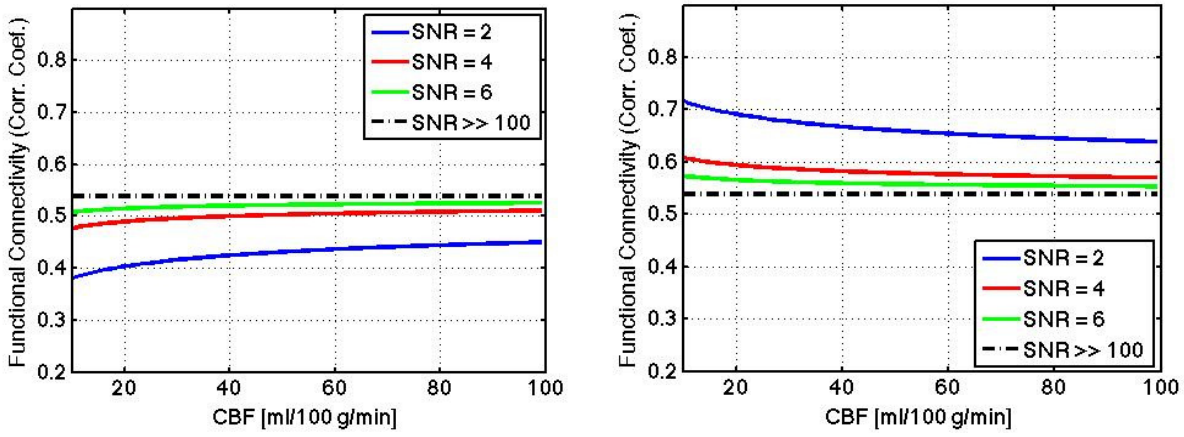

(a) **(b)**

Figure 2.1: Simulation of functional connectivity vs. resting CBF, when the correlation between two neural sources (r_s) is (a) greater and (b) less than the functional connectivity between their respective noise components (r_n).

2.3.1.2 Cerebrovascular reactivity

A positive relationship can be seen between functional connectivity and CVR when r_s is greater than r_n (Figure 2.2a) and negatively when r_s is less than r_n (Figure 2.2a), and the relationship saturates at higher CVR. The saturation starts at lower CVR when SNR increases. Similar to the case of CBF_0, there is no correlation between CVR and functional connectivity when we disregard the effect of the physiological noise.

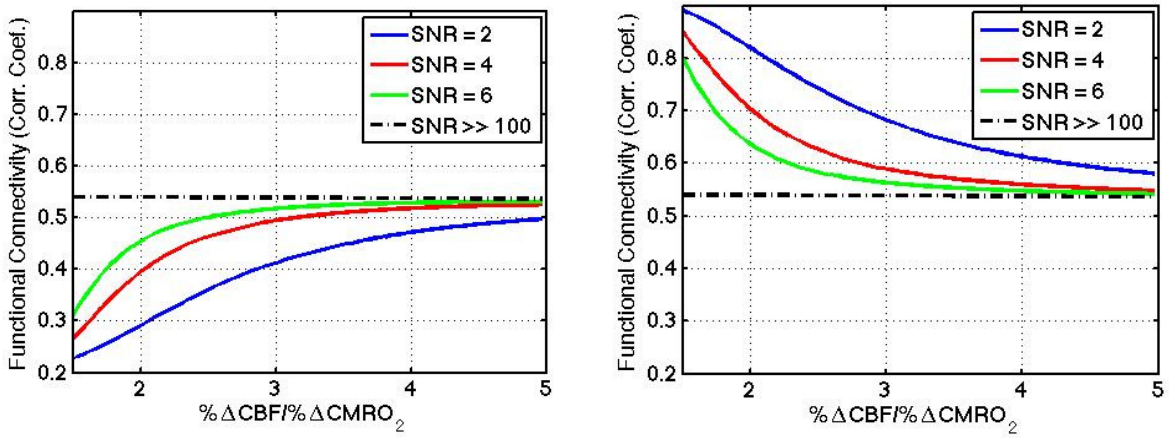

(a) **(b)**

Figure 2.2: Simulation of functional connectivity vs. CVR, which is denoted by the percent change in CBF over the percent change in CMRO2, when r_s is (a) greater and (b) less than r_n.

2.3.1.3 Venous-blood oxygenation

In contrast to CBF_0 and CVR, the relationship between functional connectivity and Y_v decreases when r_s is greater than r_n (Figure 2.3a), and increases when r_s is less than r_n (Figure 2.3b). In both cases, the relationship tends to disappear as SNR increases. Similar to the cases of CBF_0 and CVR, no correlation between Y_v and functional connectivity is seen when we disregard the effect of the physiological noise.

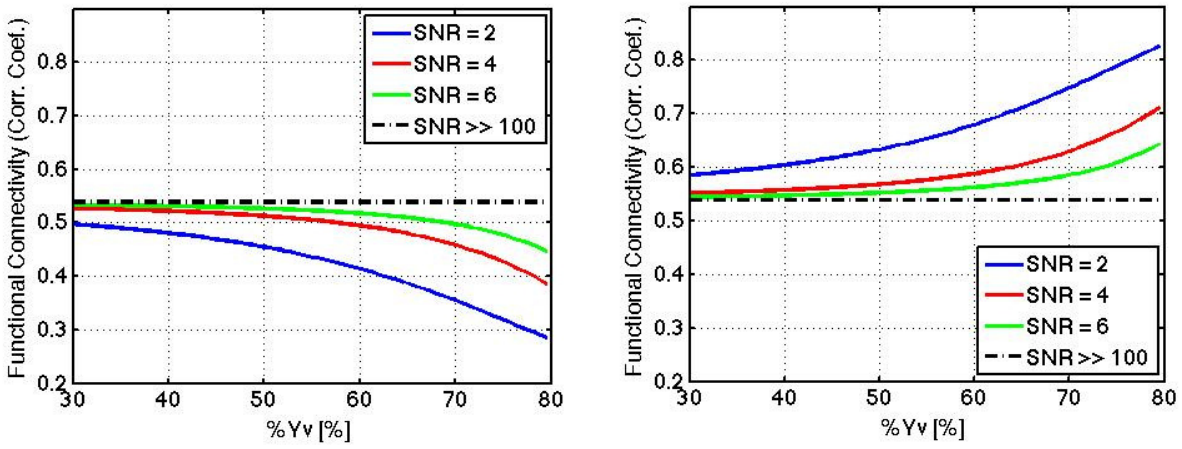

Figure 2.3: Simulation of functional connectivity vs. venous-blood oxygenation, when r_s is (a) greater and (b) less than r_n.

2.3.2 Experimental data

2.3.2.1 Inter-subject analysis

In Figure 2.4 (1st column), we illustrate rs-fMRI functional connectivity maps averaged across 15 subjects in each resting-state network. Regions with the strongest functional connectivity are shown in yellow in each case.

To demonstrate the inter-subject effect of CBF_0 on fcMRI measurements, the voxels demonstrating significant correlations with functional connectivity are shown in Figure 2.4 (2nd column) for each resting-state network. In the case of the DMN, voxels in the cingulate cortex, middle and inferior temporal gyrus, and the frontal region of the brain are associated positive correlations with CBF_0, while regions in the right lateral-parietal region indicate negative correlations. In the SMN, we also found positive fcMR-CBF_0 correlations. Lastly, for visual-network connectivity (VN), we found negative fcMRI-CBF_0 correlations.

In regards to the effect of CVR (Figure 2.4, 3rd column), in the DMN, positive correlations are found with fcMRI measurements in the angular gyrus, while negative correlations are found in the superior temporal gyrus and anterior cingulate cortex. Similar CVR effects are found in the SMN, where positive CVR-fcMRI correlations are found in the primary motor cortex. Again, in the VN, some regions in the visual cortex illustrated negative correlation between CVR and fcMRI measurements.

In regards to the effect of Y_v, again, the correlations with fcMRI measurements are predominantly positive, as shown in Figure 2.4 (4th column). In the DMN, such positive effects are mainly seen in the frontal nodes, whereas in the SMN, only a small region of the motor cortex exhibited positive correlations with Y_v. As before, mainly negative correlations are observed in the VN. As for the residual Y_v when regressing out the effect of CBF_0, as shown in Figure 2.5, no significant ROI-based relationship between residual Y_v and residual fcMRI values were observed, although the relationship is very strong in the SMN (Figure 2.5b).

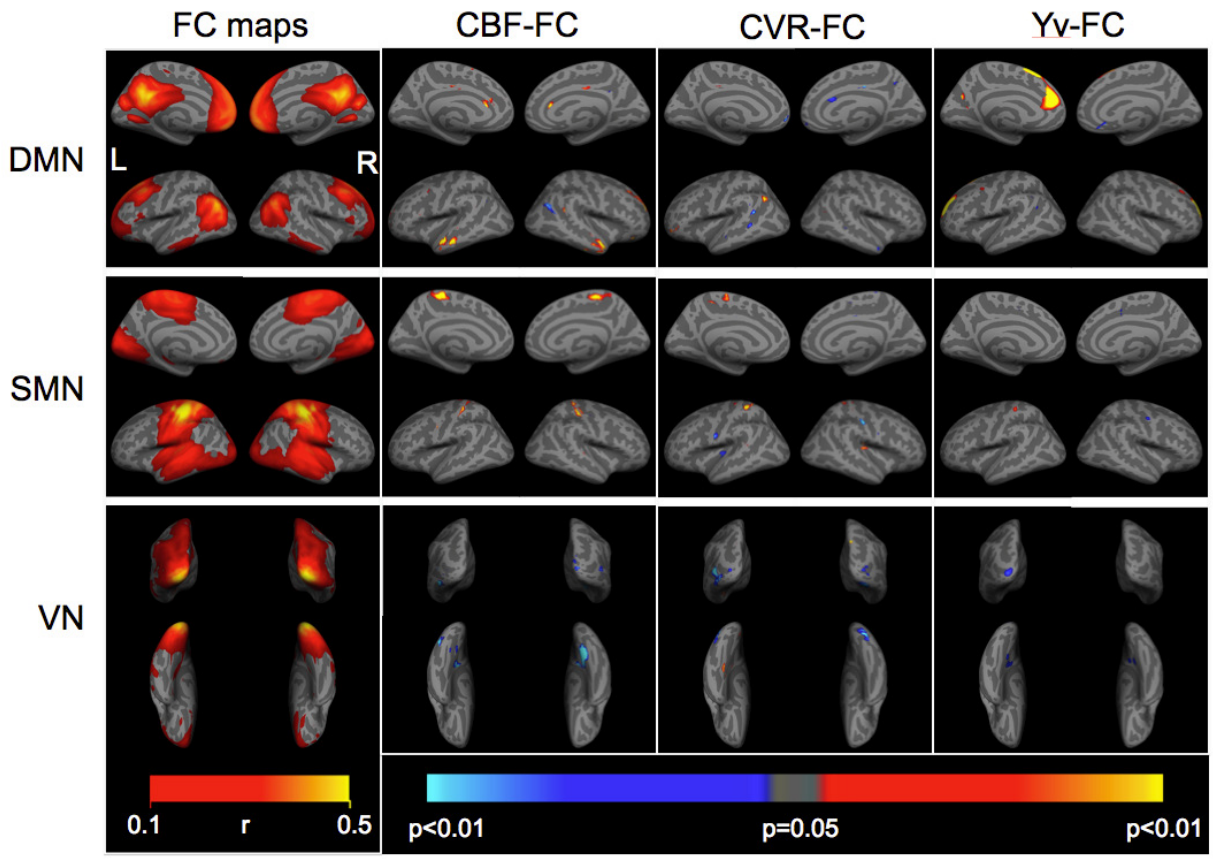

Figure 2.4: Between-subject general linear model (GLM) analysis: functional connectivity vs. CBF_0, CVR and Y_v. Column 1: group-average functional connectivity (FC) maps corresponding to the default-mode network (DMN), sensorimotor network (SMN) and the visual network (VN). Columns 2-4: statistical results association fcMRI values (correlations coefficients) with each of the three physiological variables. For the DMN and SMN, the lateral and medial cortical surfaces are shown (L: left, R: right), whereas for the VN, the caudal and ventral cortical surfaces are shown. The red-yellow regions illustrate significant positive associations, whereas blue regions represent negative associations respectively.

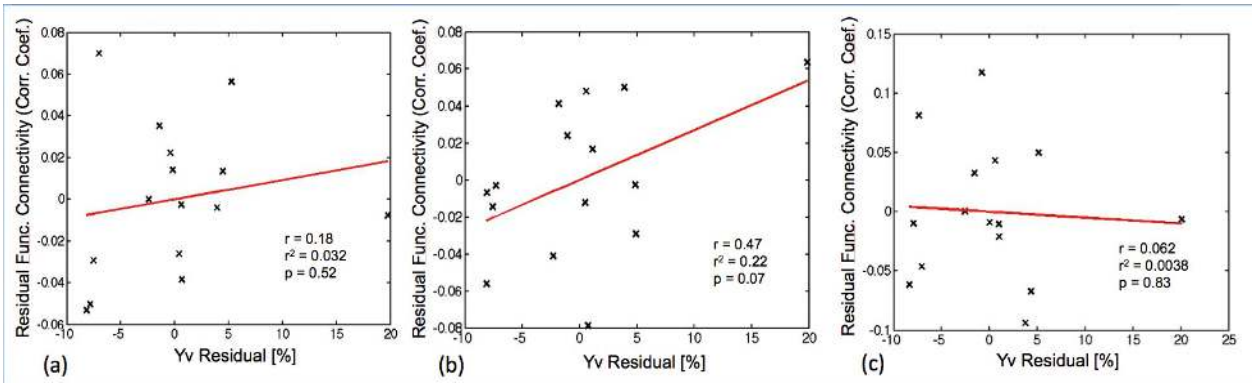

Figure 2.5: The inter-subject association between Y_v and fcMRI measurements after controlling the effect of CBF_0. After regressing the effect of CBF_0 from Y_v, we did not see any significant changes in any of the resting-state networks.

2.3.2.2 Within-subject analysis

In regards to the effect of CBF_0 on functional connectivity, the majority of subjects exhibit significant positive correlation in the default-mode network (DMN) and the sensorimotor network (SMN). However, in the visual network (VN), the majority of subjects are associated with significant negative correlations between CBF_0 and connectivity (Figure 2.6).

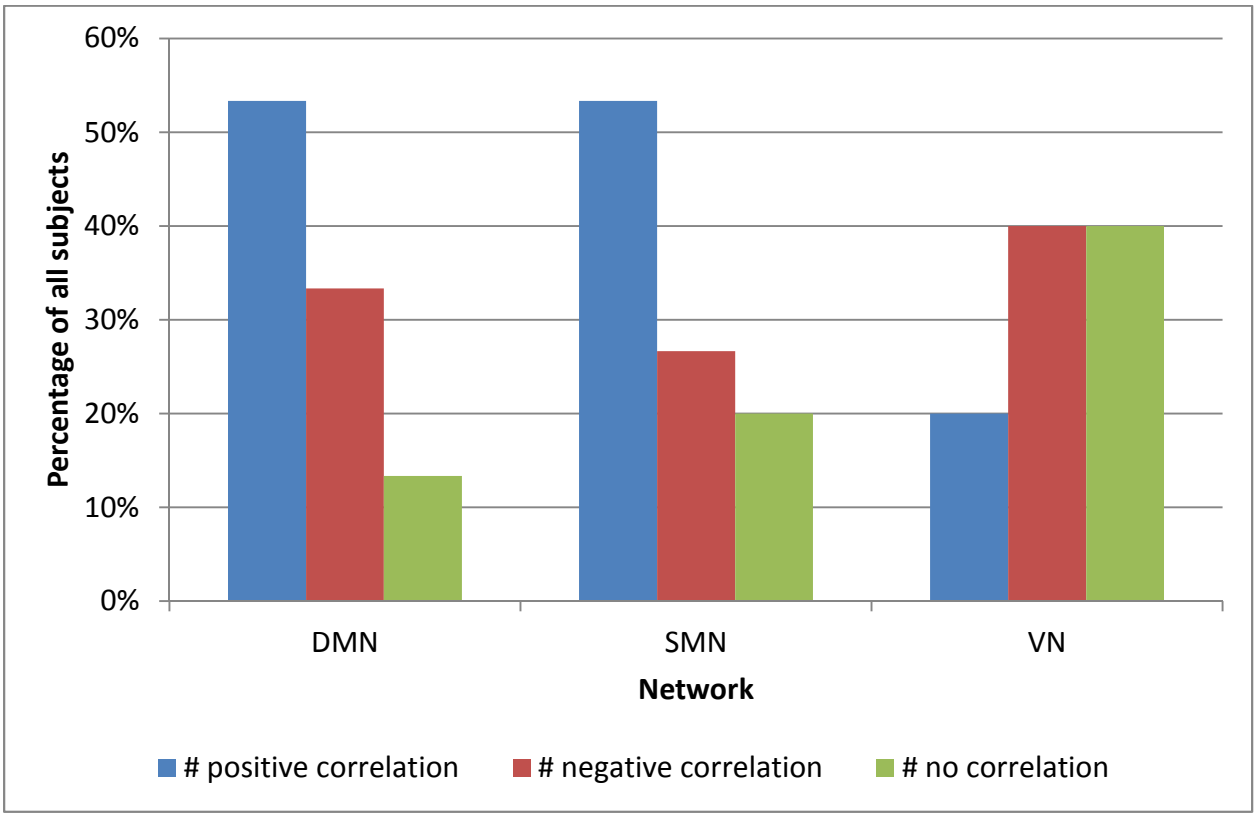

Figure 2.6: Within-subject voxel-wise analysis: correlations of functional connectivity vs. CBF_0 in the default-mode network (DMN), sensorimotor network (SMN), and the visual network (VN). These results are based on significant correlations alone.

In terms of CVR, unlike for CBF_0, the majority of subjects display either negative or no correlation between CVR and fcMRI measurements in the DMN and SMN. However, in the VN, the primary association between CVR and fcMRI is positive (Figure 2.7).

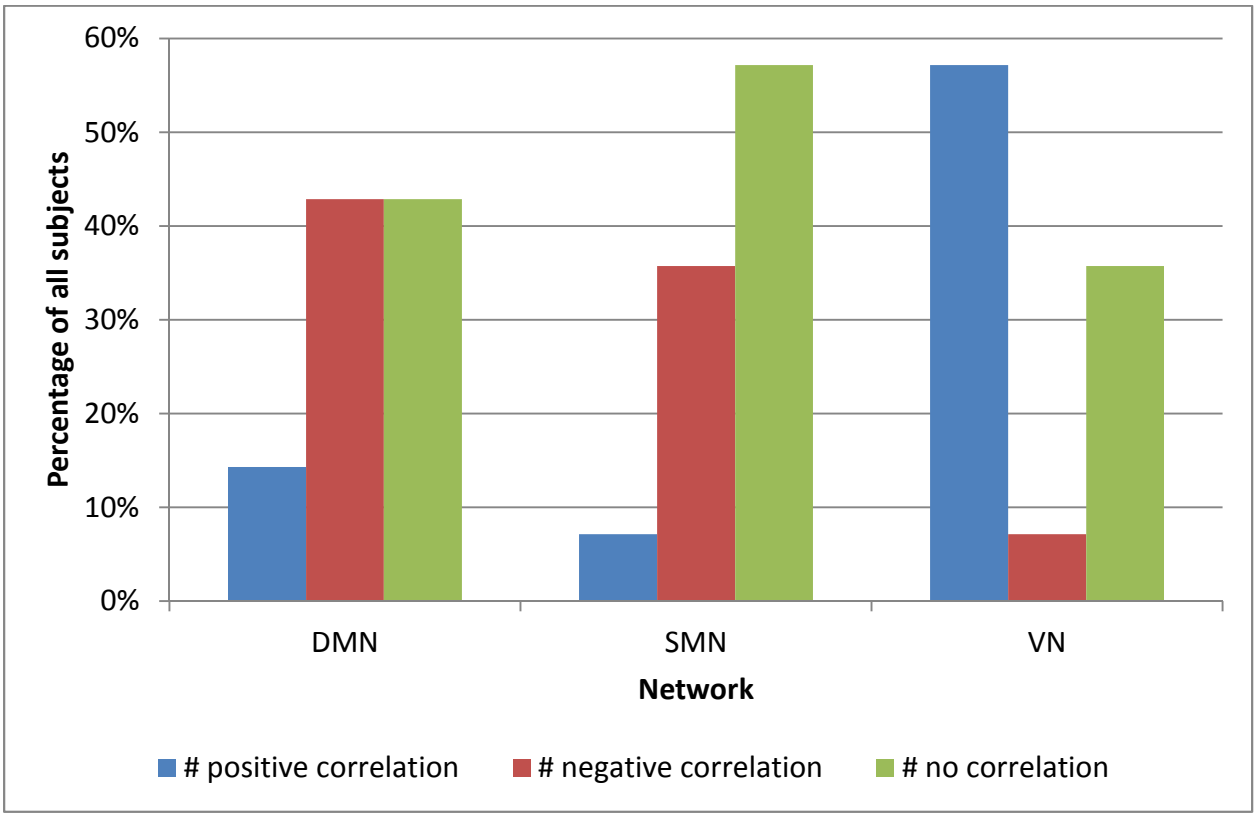

Figure 2.7: Within-subject voxel-wise analysis: correlations of functional connectivity vs. CVR in the default-mode network (DMN), sensorimotor network (SMN), and the visual network (VN).

2.4 Discussion

Resting-state fMRI functional connectivity (fcMRI) measurements are often found to be highly variable across subjects, and even across scans of the same subject. Previous work (Liu, Hebrank et al. 2013) demonstrated that task-related fMRI responses are significantly associated with physiological modulators such as resting cerebral blood flow (CBF_0), cerebrovascular reactivity (CVR) and venous-blood oxygenation (Y_v). This motivated our study of similar physiological modulators in fcMRI. In this study, we demonstrate that these same modulators indeed have a

significant impact on resting-state fcMRI measurements. Importantly, we used a simulation-guided empirical approach to probe and understand the biophysical underpinnings of this impact.

2.4.1 Resting cerebral blood flow (CBF_0)

As shown in our simulations, when physiological-noise induced correlations (r_n) do not dominate, fcMRI measurements are positively correlated with CBF_0. For the most part, this was the case in the experimental results. When examining across subjects, fcMRI measurements are positively correlated in the precentral gyrus, cingulate cortex and frontal cortex (lateral and medial), and negatively correlated with CBF_0 only in small parts of the lateral parietal lobe. This predominantly positive effect of CBF_0 is carried over into the within-subject results, in which the majority of subjects exhibit positive voxel-wise correlation between CBF_0 and fcMRI measurements. While this positive trend is in agreement with previous studies (Liang, Zou et al. 2013), and has been suggested to indicate that regions exhibiting higher connectivity are also those associated with higher resting metabolism, hence higher CBF_0 (Liang, Zou et al. 2013). However, the inter-subject variability in this effect is also informative.

As our simulations showed, the relationship between CBF_0 and functional connectivity heavily depends on the relationship between the value of r_s and r_n. Specifically, based on our assumptions, CBF_0 and fcMRI measurements would be negative correlated when physiological-noise related correlations dominate over "neuronally driven" correlations. Given the highly structured nature of physiological noise effects (Chang and Glover 2009a, Chang and Glover 2009b, Golestani, Chang et al. 2015), it is conceivable that different regions are associated with different levels of physiological-noise contribution to the rs-fMRI signal. Moreover, it is well established that these noise effects are highly variable across subjects (Chang and Glover 2009a,

Golestani, Chang et al. 2015), potentially due to differences in vascular physiology (Lu, Zhao et al. 2008) and positioning inside the scanner (Khatamian and Chen 2013). Thus, the physiological modulation of fcMRI measurements should ideally be corrected in a subject- and regionally specific manner. Moreover, the visual network differs in behaviour from the DMN and SMN, in both between- and within-subject analysis. We note that the visual network is associated with particularly high vascular density (Cavaglia, Dombrowski et al. 2001) hence perfusion, which may have contributed to its singular behaviour. In fact, as seen in the simulations (Figure 2.1), this may lead to a scenario in which physiological-noise driven correlations dominate, as illustrated in Figure 2.1b.

2.4.2 Cerebrovascular reactivity

In the group-wise results, the correlation between fcMRI and CVR measurements is mainly positive in the most strongly correlated regions of the DMN and SMN. This is consistent with our previous group-wise findings in resting-state fMRI (Golestani, Kwinta et al. 2016), as well as with findings based on task-based fMRI, in that the task response was positively correlated with CVR (Liu, Hebrank et al. 2013). However, negative fcMRI-CVR correlations were observed in the VN, as well as sporadically in the DMN and SMN, highlighting regional variability in this relationship. Furthermore, in the within-subject results, the majority of subjects demonstrated negative or lack of voxel-wise CVR-fcMRI correlations in the DMN and SMN. We note that while the group-wise results reflect only the voxels exhibiting the most consistent CVR effect across subjects, the within-subject results need not follow the same trend. In fact, as mentioned earlier, physiology and physiological-noise effects differ across subjects and brain regions. Moreover, the detectability of CVR modulation of fcMRI values depends on the variability in

CVR as well as in fcMRI measurements themselves. CVR variability within each ROI depends on the network being examined, and likely to differ between subjects. These various modulators are likely all to contribute to the large inter-subject variability in the individual voxel-wise results. Lastly, as shown in our simulations (Figure 2.2), higher CVR is associated with reduced CVR-sensitivity in fcMRI measurements, either positive or negative. This is particularly true in the visual cortex, and may underline the inconsistency in fcMRI-CVR associations between the VN and the remaining networks.

2.4.3 Venous-blood oxygenation

Given the previously described link between Y_v and CBF_0, we expected that a portion of the fcMRI-Y_v relationship would be influenced by CBF_0. Indeed, in the group analysis, fcMRI and Y_v are positive correlated, particularly in the DMN. However, the effect of Y_v from a single blood vessel (the sagittal sinus) appears more extensive than those of CBF_0. This may be due in part to differences in measurement variability of Y_v and of CBF_0, but also reflect that Y_v may not be fully accounted for by CBF_0. Indeed, even after regressing the effects of CBF_0 from Y_v, we still observed a near-significant effect of residual Y_v on the residual fcMRI values. We trust that with a large sample and potentially more localized Y_v measurements, we should be able to demonstrate a significant relationship between Y_v and fcMRI that is independent of CBF_0.

2.5 Recommendations

This study demonstrates through theoretical and empirical evidence that systemic physiological differences significantly contribute to variations in rs-fcMRI measurements. While these contributions are subject- and regionally specific, it is important to note that these are not neuronal-specific physiological modulators, and thus their modulation of fcMRI measurements

represents confounds that are likely to reduce the power of group analysis in the rs-fMRI context.

It is important to note that the impact of these modulators differs across individuals and across brain regions, and that appropriate correction would require additional scans within the same session as the fcMRI scan. However, if scan time is a concern, the simulations indicate that, within the natural range of variation for each of the physiological modulators in this work, CVR and Y_v have the strongest impact on fcMRI measurements, consistent with the experimental results, suggesting that it is more important to correct these than for CBF_0.

The simulation results indicate that physiological noise effects play an important role in altering the effects of the physiological modulators on functional connectivity measurements. In fact, the physiological modulations associated with $r_n > r_s$ have the opposite effect from those seen when $r_n < r_s$, and this greatly increases the variability of physiological effects. Although not examined in this work, alternative ways to reduce physiological noise include independent component analysis (ICA), which can segregate each subject's rs-fMRI time-series data into a linear mixture of independent non-Gaussian components (Beckmann and Smith 2004). Here, noise reduction is model independent, and by assuming that the physiological noise components are independent from the functionally relevant data, one can potentially further reduce the contribution of noise effects. Recently proposed methods include ICA-AROMA and FSL-FIX, which aim to capture noise components based on automatically classifying signal components as noise and non-noise based on a set of a priori features (Griffanti, Salimi-Khorshidi et al. 2014, Pruim, Mennes et al. 2015).

2.6 Potential Caveats

We assumed that the BOLD-signal model that was derived from steady-state BOLD also applies to resting-state BOLD. We are aware that this may be an oversimplification, and that this model has not been explicitly validated for resting-state BOLD. Nonetheless, this model was previously used in other rs-fMRI studies (Fukunaga, Horovitz et al. 2008, Wu, Gu et al. 2009) to provide a basic biophysical framework to guide our understanding of the physiological nature of the resting-state BOLD signal. In our future work, we hope to refine and experimentally demonstrate the accuracy of this model for rs-fMRI.

Moreover, as indicated earlier, we were unable to obtain spatially resolved measurements of Y_v, as our method limited us to singularly large veins. This was the case in earlier studies of a similar nature (Lu, Xu et al. 2011, Liu, Hebrank et al. 2013). Nonetheless, we also note that oxygen-extraction fraction, which is complimentary to Y_v, is much more uniform across the brain than CVR and CBF_0 (Hyder, Herman et al. 2016). Thus, we do not expect large differences between global and regional Y_v.

In this work, the effect of each physiological modulator on functional connectivity is relatively weak, potentially due to the fact that all subjects are young adults. If we were to conduct a research on a larger population with a larger age range, we are likely to see a larger variability in CBF_0, Y_v, and CVR, and this would lead to more apparent effects on functional connectivity.

Another potential limitation is the uneven ratio in sex and age of the subjects participated in this research. Out of 15 subjects, 9 subjects (60 %) are female, and there are 12 subjects in the age group of 18-27, while 2 subjects in the 30s and 1 subject in the 40s age group. A more evenly

distributed subject population in both sex and age may yield more consistent results on the effects of physiological modulators on functional connectivity.

Lastly, we have not experimentally verified the outcomes of our simulations. To do so, one option is to modulate the effect of each physiological modulator in each subject through established maneuvers. This will be pursued in our future research.

2.7 Conclusion

In this study, we have illustrated that the physiological effects, namely the resting CBF (CBF_0), venous-blood oxygenation (Y_v), and the cerebral-vascular reactivity (CVR), have a significant impact on resting-state fMRI-based functional connectivity measurements in multiple resting-state networks. However, the effects are regionally specific. In addition, different individuals exhibited different physiological effects. Minimizing these physiological effects would allow us to examine functional connectivity of the true signals between brain regions, and that enables researchers to understand more about functional connectivity.

Chapter 3

Future Directions

In the previous chapter, through simulations and experiments, it was shown that the physiological parameters have significant effects on resting-state functional connectivity. When examining across subjects, there were regions that exhibited significant positive correlations between rs-fMRI functional connectivity measurements and the physiological parameters, namely the resting cerebral blood flow (CBF_0), venous-blood oxygenation (Y_v), and cerebrovascular reactivity (CVR). In addition, as shown in simulation, each physiological parameter is associated with a different relationship with functional connectivity, largely depending on the relationship between the correlation of true signals (r_s) and the correlation of physiological noise components (r_n) among the brain regions. The experimental results have illustrated that different brain regions can exhibit different levels of physiological noise, and that the effects vary across subjects as well. Thus, to understand fully on the effect of the physiological parameters, we need to better understand the physiological noise component across the brain.

3.1 Origins of variability in physiological modulation of rs-fcMRI measurements

One of the key findings of this work is that the dependence of rs-fcMRI measurements depends on the relative strengths of neuronal- and physiological noise-driven correlations (i.e. r_s and r_n). Previous studies have documented that two main physiological noise factors contribute to the rs-fMRI signal variability, respiratory and cardiac responses (Birn, Diamond et al. 2006, Shmueli, van Gelderen et al. 2007, de Munck, Gonçalves et al. 2008, Golestani, Chang et al. 2015). Golestani *et al.* (Golestani, Chang et al. 2015) have illustrated that the effect of variability in respiration on rs-fMRI signal is more prominent in the occipital and frontal cortical areas, while cardiac effects are more apparent in the white matter and borders with cerebrospinal fluid. This suggests that different regions experience different effects from these physiological factors. Thus, the correlation induced by physiological noise, primarily respiratory and cardiac noise, varies from region to region, and that may underlie the spatial variability found in this work in terms of the effects of physiological modulators, namely CBF_0, Y_v, and CVR. To test this theory, we can regress out the effect of the physiological effects of cardiac and respiratory responses from rs-fMRI signal and then re-examine the relationships of the CBF_0, Y_v, and CVR with functional connectivity.

The effect of respiratory and cardiac responses on rs-fMRI not only varies from region to region, but they also vary across subjects. Specifically, we found that different subjects can exhibit opposite effects of physiological modulators. As pointed out in (Peng, Niazy et al. 2013, Golestani, Chang et al. 2015), the level of arousal and vigilance can significantly influence the physiological factors. Thus, this creates a rs-fMRI variability of between 5% to over 24%, depending on the subject (Golestani, Chang et al. 2015).

Another contribution to regional variability in physiological effects may be the differences in vascular densities across the brain region. Different subjects have different vascular density as well, contributing to inter-subject rs-fMRI variability. Brain regions with more dense vasculature tend to have higher blood flow and reactivity. The occipital lobe and the precuneus region not only have the most dense vasculature (Cavaglia, Dombrowski et al. 2001), but they also have high resting oxidative metabolism (Buckner, Snyder et al. 2005) and high baseline blood flow (Chen, Rosas et al. 2011). On the other hand, according to the simulation results in the previous chapter, the impact of physiological modulators on resting-state functional connectivity diminishes as the values of the modulators increase. For instance, the relationship between functional connectivity (correlation coefficient) approaches an asymptotic value when CBF_0 is very high. This means that regions with higher vascular density would have less correlation. Thus, in future work, instead of examining functional connectivity in each resting-state network, we can examine the brain by separating regions based on their vascular densities to see whether subject with higher vascular density in a particular region has less correlation between functional connectivity and the physiological parameters.

3.2 Larger sample size

Results obtained in this experiment were based on 15 healthy subjects, which is a limitation in this thesis. However, studies with larger sample sizes produced similar result (Li, Zhu et al. 2012, Liang, Zou et al. 2013).

3.3 Other resting-state networks

In this study we examined the relationship between physiological parameters and resting-state functional connectivity and deduced that there are differences across various resting-state

networks, in particular the results within the visual network in comparison to the sensorimotor and motor networks. Thus, we should also examine other resting-state networks, such as the executive control, limbic, and fronto-parietal networks, to see the similarities and differences of the effects of physiological parameters across resting-state networks. In addition, as mentioned previously, voxel-to-voxel connectivity that is independent from resting-state networks can be performed to examine the effect of the physiological parameters across all brain regions, similar to the study carried out by (Liang, Zou et al. 2013).

3.4 Validation of the results

Furthermore, in this experiment, the analysis was carried out in MNI space coordinate to match with the space of resting-state functional connectivity maps. While this is desirable to inspect visually different parametric maps across all subjects, two-step transformation was performed on the CBF and CVR maps. More approximations were carried out in multiple transformations, and that may compromise the measured signals. Thus, we should verify the results obtained in this experiment by performing only one-step transformation. This can be done by performing transformations on CBF, CVR, and resting-state functional connectivity maps into the high-resolution anatomical space. In this way only one-step transformation is carried out across all data, and that minimizes the error incurred from transformations.

References

1. Ashburner, J. and K. J. Friston (2005). "Unified segmentation." Neuroimage **26**: 839-851.
2. Balduzzi, D., B. A. Riedner and G. Tononi (2008). "A BOLD window into brain waves." Proc Natl Acad Sci U S A **105**: 15641-15642.
3. Becker, J. T., M. A. Mintun, K. Aleva, M. B. Wiseman, T. Nichols and S. T. Dekosky (1996). "Alterations in functional neuroanatomical connectivity in Alzheimer's disease. Positron emission tomography of auditory verbal short-term memory." Ann N Y Acad Sci **777**: 239-242.
4. Beckmann, C. F. and S. M. Smith (2004). "Probabilistic independent component analysis for functional magnetic resonance imaging." IEEE Trans Med Imaging **23**: 137-152.
5. Billett, H. H. (1990). Hemoglobin and Hematocrit. Clinical Methods: The History, Physical, and Laboratory Examinations. H. K. Walker, W. D. Hall and J. W. Hurst. Boston, Butterworths.
6. Birn, R. M., J. B. Diamond, M. A. Smith and P. A. Bandettini (2006). "Separating respiratory-variation-related fluctuations from neuronal-activity-related fluctuations in fMRI." NeuroImage **31**: 1536-1548.
7. Birn, R. M., M. A. Smith, T. B. Jones and P. A. Bandettini (2008). "The respiration response function: the temporal dynamics of fMRI signal fluctuations related to changes in respiration." Neuroimage 40(2): 644-654.
8. Biswal, B., A. G. Hudetz, F. Z. Yetkin, V. M. Haughton and J. S. Hyde (1997). "Hypercapnia reversibly suppresses low-frequency fluctuations in the human motor cortex during rest using echo-planar MRI." J Cereb Blood Flow Metab **17**: 301–308.
9. Biswal, B., F. Z. Yetkin, V. M. Haughton and J. S. Hyde (1995). "Functional connectivity in the motor cortex of resting human brain using echo-planar MRI." Magn Reson Med **34**(4): 537-541.
10. Blockley, N. P., I. D. Driver, S. T. Francis, J. A. Fisher and P. A. Gowland (2011). "An improved method for acquiring cerebrovascular reactivity maps." Magn Reson Med **65**: 1278–1286.
11. Bollen, K. A. and R. W. Jackman (1990). Regression Diagnostics: An Expository Treatment of Outliers and Influential Cases. In *Modern Methods of Data Analysis*. Newbury Park, CA, Sage.
12. Buckner, R. L., A. Z. Snyder, B. J. Shannon, G. LaRossa, R. Sachs, A. F. Fotenos, Y. I. Sheline, W. E. Klunk, C. A. Mathis, J. C. Morris and M. A. Mintun (2005). "Molecular, structural, and functional characterization of Alzheimer's disease: evidence for a relationship between default activity, amyloid, and memory." J Neurosci **25**(34): 7709-7717.
13. Buxton, R. B., K. Uludag, D. J. Dubowitz and T. T. Liu (2004). "Modeling the hemodynamic response to brain activation." NeuroImage **23**: S220-233.
14. Cavaglia, M., S. M. Dombrowski, J. Drazba, A. Vasanji, P. M. Bokesch and D. Janigro (2001). "Regional variation in brain capillary density and vascular response to ischemia." Brain Res **910**(1-2): 81-93.
15. Chang, C. and G. H. Glover (2009a). "Effects of model-based physiological noise correction on default mode network anti-correlations and correlations." Neuroimage **47**(4): 1448-1459.
16. Chang, C. and G. H. Glover (2009b). "Relationship between respiration, end-tidal CO2, and BOLD signals in resting-state fMRI." NeuroImage **47**: 1381-1393.

17. Chen, J. J. and G. B. Pike (2009). "BOLD-specific cerebral blood volume and blood flow changes during neuronal activation in humans." NMR Biomed **22**(10): 1054-1062.
18. Chen, J. J. and G. B. Pike (2010). "Global cerebral oxidative metabolism during hypercapnia and hypocapnia in humans: implications for BOLD fMRI." J Cereb Blood Flow Metab **30**: 1094-1099.
19. Chen, J. J. and G. B. Pike (2010). "MRI measurement of the BOLD-specific flow-volume relationship during hypercapnia and hypocapnia in humans." NeuroImage **53**: 383-391.
20. Chen, J. J., H. D. Rosas and D. Salat (2011). "Age-associated reductions in cerebral blood flow are independent from regional atrophy." NeuroImage **55**: 468-478.
21. Chen, Y. and T. B. Parrish (2009). "Caffeine's effects on cerebrovascular reactivity and coupling between cerebral blood flow and oxygen metabolism." NeuroImage **44**(3): 647-652.
22. Chiarelli, P. A., D. P. Bulte, D. Gallichan, S. K. Piechnik, R. Wise and P. Jezzard (2007). "Flow-metabolism coupling in human visual, motor, and supplementary motor areas assessed by magnetic resonance imaging." Magn Reson Med **57**: 538–547.
23. Cohen, E. R., K. Ugurbil and S. G. Kim (2002). "Effect of basal conditions on the magnitude and dynamics of the blood oxygenation level-dependent fMRI response." J Cereb Blood Flow Metab **22**(9): 1042-1053.
24. Cordes, D., V. M. Haughton, K. Arfanakis, J. D. Carew, P. A. Turski, C. H. Moritz, M. A. Quigley and M. E. Meyerand (2001). "Frequencies contributing to functional connectivity in the cerebral cortex in "resting-state" data." AJNR American journal of neuroradiology **22**(7): 1326-1333.
25. Damoiseaux, J. S., C. F. Beckmann, E. J. Sanz Arigita, F. Barkhof, P. Scheltens, C. J. Stam, S. M. Smith and S. A. Rombouts (2008). "Reduced resting-state brain activity in the default network in normal aging." Cereb Cortex **18**: 1856-1864.
26. Davis, T. L., K. K. Kwong, R. M. Weisskoff and B. R. Rosen (1998). "Calibrated functional MRI: Mapping the dynamics of oxidative metabolism." Proc Natl Acad Sci U S A **95**: 1834-1839.
27. de Munck, J. C., S. I. Gonçalves, T. J. Faes, J. P. Kuijer, P. J. Pouwels, R. M. Heethaar and F. H. Lopes da Silva (2008). "A study of the brain's resting state based on alpha band power, heart rate and fMRI." Neuroimage **42**(1): 112-121.
28. D'esposito, M., E. Zarahn, G. K. Aguirre and B. Rypma (1999). "The effect of normal aging on the coupling of neural activity to the bold hemodynamic response." NeuroImage **10**(1): 6-14.
29. Finnerty, G. T. and J. G. Jefferys (1993). "Functional connectivity from CA3 to the ipsilateral and contralateral CA1 in the rat dorsal hippocampus." Neuroscience **56**(1): 101-108.
30. Fox, M. D. and M. Greicius (2010). "Clinical applications of resting state functional connectivity." Front Syst Neurosci **4**(19): 1-13.
31. Fox, M. D., A. Z. Snyder, J. L. Vincent, M. Corbetta, D. C. Van Essen and M. E. Raichle (2005). "The human brain is intrinsically organized into dynamic anticorrelated functional networks." PNAS Proc Nat Aca Sci USA **102**: 9673-9678.
32. Friston, K. J., A. P. Holmes, K. J. Worsley, J.-B. Poline, C. D. Frith and R. S. J. Frackowiak (1995). "Statistical parametric maps in functional imaging: A general linear approach." Human Brain Mapping **2**: 189-210.

33. Friston, K. J., C. D. Frith, P. F. Liddle and R. S. Frackowiak (1993). "Functional connectivity: the principal-component analysis of large (PET) data sets." J Cere Blood Flow Metab **13**(1): 5-14.
34. Fukunaga, M., S. G. Horovitz, J. A. de Zwart, P. van Gelderen, T. J. Balkin, A. R. Braun and J. H. Duyn (2008). "Metabolic origin of BOLD signal fluctuations in the absence of stimuli." J Cereb Blood Flow Metab **28**(7): 1377-1387.
35. Glover, G. H. (1999). "Deconvolution of impulse response in event-related BOLD fMRI." Neuroimage **9**(4): 416-429.
36. Golestani, A. M., C. Chang, J. B. Kwinta, Y. B. Khatamian and J. Jean Chen (2015). "Mapping the end-tidal CO2 response function in the resting-state BOLD fMRI signal: spatial specificity, test-retest reliability and effect of fMRI sampling rate." Neuroimage **104**: 266-277.
37. Golestani, A. M., J. B. Kwinta, S. C. Strother, Y. B. Khatamian and J. J. Chen (2016). "The association between cerebrovascular reactivity and resting-state fMRI functional connectivity in healthy adults: The influence of basal carbon dioxide." NeuroImage **132**: 301-313.
38. Greicius, M. D., B. Krasnow, A. L. Reiss and V. Menon (2003). "Functional connectivity in the resting brain: a network analysis of the default mode hypothesis." Proc Natl Acad Sci U S A **100**(1): 253-258.
39. Griffanti, L., G. Salimi-Khorshidi, C. F. Beckmann, E. J. Auerbach, G. Douaud, C. E. Sexton, E. Zsoldos, K. P. Ebmeier, N. Filippini, C. E. Mackay, S. Moeller, J. Xu, E. Yacoub, G. Baselli, K. Ugurbil, K. L. Miller and S. M. Smith (2014). "ICA-based artefact removal and accelerated fMRI acquisition for improved resting state network imaging." Neuroimage **95**: 232-247.
40. Grubb, R. L. J., M. E. Raichle, J. O. Eichling and M. M. Ter-Pogossian (1974). "The effects of changes in PaCO2 on cerebral blood volume, blood flow, and vascular mean transit time." Stroke **5**(5): 630-639.
41. Hoffstaedter, F., C. Grefkes, S. Caspers, C. Roski, N. Palomero-Gallagher, A. R. Laird, P. T. Fox and S. B. Eickhoff (2014). "The role of anterior midcingulate cortex in cognitive motor control: evidence from functional connectivity analyses." Hum Brain Mapp **35**(6): 2741-2753.
42. Hoge, R. D. (2012). "Calibrated FMRI." Neuroimage **62**(2): 930-937.
43. Hoge, R. D., J. Atkinson, B. Gill, G. R. Crelier, S. Marrett and G. B. Pike (1999). "Investigation of BOLD signal dependence on cerebral blood flow and oxygen consumption: the deoxyhemoglobin dilution model." Magn Reson Med **42**(5): 849-863.
44. Hyder, F., P. Herman, C. J. Bailey, A. Møller, R. Globinsky, R. K. Fulbright, D. L. Rothman and A. Gjedde (2016). "Uniform distributions of glucose oxidation and oxygen extraction in gray matter of normal human brain: No evidence of regional differences of aerobic glycolysis." J Cere Blood Flow Metab.
45. Ito, H., I. Kanno, M. Ibaraki, J. Hatazawa and S. Miura (2003). "Changes in human cerebral blood flow and cerebral blood volume during hypercapnia and hypocapnia measured by positron emission tomography." J Cereb Blood Flow Metab **23**(6): 665-670.
46. Jain, V., M. C. Langham, T. F. Floyd, G. Jain, J. F. Magland and F. W. Wehrli (2011). "Rapid magnetic resonance measurement of global cerebral metabolic rate of oxygen consumption in humans during rest and hypercapnia." J Cere Blood Flow Metab **31**: 1504–1512.

47. Jensen, J. H. and R. Chandra (2000). "NMR relaxation in tissues with weak magnetic inhomogeneities." Magn Reson Med **44**(1): 144-156.
48. Kannurpatti, S. S., M. A. Motes, B. Rypma and B. B. Biswal (2011). "Non-neural BOLD variability in block and event-related paradigms." Magn Reson Imaging. **29**: 140-146.
49. Kastrup, A., T. Q. Li, G. Kruger, G. H. Glover and M. M. E (1999). "Relationship between cerebral blood flow changes during visual stimulation and baseline flow levels investigated with functional MRI." Neuroreport **10**(8): 1751-1756.
50. Kety, S. S. and C. F. Schmidt (1948). "The effects of altered arterial tensions of carbon dioxide and oxygen on cerebral blood flow and cerebral oxygen consumption of normal young men." J Clin Invest **27**(4): 484-492.
51. Khalili-Mahani, N., M. J. van Osch, M. de Rooij, C. F. Beckmann, M. A. van Buchem, A. Dahan, J. M. van Gerven and S. A. Rombouts (2012). "Spatial heterogeneity of the relation between resting-state connectivity and blood flow: an important consideration for pharmacological studies." Hum Brain Mapp **35**(3): 929-942.
52. Khatamian, Y. and J. J. Chen (2013). Respiratory effects in resting state fMRI: a comparison of respiration measurement techniques. Org Hum Brain Mapp. Seattle**:** 3478.
53. Koles, Z. J. and P. Flor-Henry (1987). "The effect of brain function on coherence patterns in the bipolar EEG." Int J Psychophysiol. **5**(1): 63-71.
54. Leblanc, R., J. L. Tyler, G. Mohr, E. Meyer, M. Diksic, L. Yamamoto, L. Taylor, S. Gauthier and A. Hakim (1987). "Hemodynamic and metabolic effects of cerebral revascularization." J Neurosurg **66**(4): 529-535.
55. Li, Z., Y. Zhu, A. R. Childress, J. A. Detre and Z. Wang (2012). "Relations between BOLD fMRI-Derived Resting Brain Activity and Cerebral Blood Flow." PLoS One **7**(9): e44556.
56. Liang, X., Q. Zou, Y. He and Y. Yang (2013). "Coupling of functional connectivity and regional cerebral blood flow reveals a physiological basis for network hubs of the human brain." PNAS Proc Nat Aca Sci USA **110**(5): 1929-1934.
57. Liau, J. and T. T. Liu (2009). "Inter-subject variability in hypercapnic normalization of the BOLD fMRI response." NeuroImage **45**: 420-430.
58. Lin, M., H. C. Lucas Jr. and G. Shmueli (2012). "Too Big to Fail: Large Samples and the p-Value Problem." Information Syst Res: 906-917.
59. Lindauer, U., U. Dirnagl, M. Fuchtemeier, C. Bottiger, N. Offenhauser, C. Leithner and G. Royl (2010). "Pathophysiological interference with neurovascular coupling – when imaging based on hemoglobin might go blind." Front Neuroenergetics **2**(25): 1-9.
60. Liu, P., A. C. Hebrank, K. M. Rodrigue, K. M. Kennedy, D. C. Park and H. Lu (2013). "A comparison of physiologic modulators of fMRI signals." Hum Brain Mapp **34**(9): 2078-2088.
61. Liu, P., H. Huang, N. Rollins, L. F. Chalak, T. Jeon, C. Halovanic and H. Lu (2014). "Quantitative assessment of global cerebral metabolic rate of oxygen (CMRO2) in neonates using MRI." NMR Biomed **27**(3): 332-340.
62. Liu, T. T. (2013). "Neurovascular factors in resting-state functional MRI." NeuroImage **80**: 339-348.
63. Lu, H., C. Zhao, Y. Ge and K. Lewis-Amezcua (2008). "Baseline Blood Oxygenation Modulates Response Amplitude: Physiologic Basis for Intersubject Variations in Functional MRI Signals." Magn Reson Med **60**(2): 364-372.

64. Lu, H., F. Xu, K. M. Rodrigue, K. M. Kennedy, Y. Cheng, B. Flicker, A. C. Hebrank, J. Uh and D. C. Park (2011). "Alterations in Cerebral Metabolic Rate and Blood Supply across the Adult Lifespan." Cereb Cortex **21**: 1426-1434.
65. Lu, H., U. S. Yezhuvath and G. Xiao (2010). "Improving fMRI sensitvity by normalization of basal physiologic state." Hum Brain Mapp **31**: 80-87.
66. Maandag, N. J., D. Coman, B. G. Sanganahalli, P. Herman, A. J. Smith, H. Blumenfeld, R. G. Shulman and F. Hyder (2007). "Energetics of neuronal signaling and fMRI study." Proc Natl Acad Sci U S A **104**(51): 20546-20551.
67. Maggio, P., A. S. Salinet, T. G. Robinson and R. B. Panerai (2014). "Influence of CO2 on neurovascular coupling: interaction with dynamic cerebral autoregulation and cerebrovascular reactivity." Physiol Rep **2**(3): e00280.
68. Mennes, M., C. Kelly, S. Colcombe, F. X. Castellanos and M. P. Milham (2013). "The extrinsic and intrinsic functional architectures of the human brain are not equivalent." Cereb Cortex **23**(1): 223-229.
69. Nagdyman, N., T. Fleck, S. Schubert, P. Ewert, B. Peters, P. E. Lange and H. Abdul-Khaliq (2005). "Comparison between cerebral tissue oxygenation index measured by near-infrared spectroscopy and venous jugular bulb saturation in children." Intensive Care Med **31**(6): 846-850.
70. Nasrallah, F. A., L. Y. Yeow, B. Biswal and K.-H. Chuang (2015). "Dependence of BOLD signal fluctuation on arterial blood CO2 and O2: Implication for resting-state functional connectivity." NeuroImage **117**: 29–39.
71. Ogawa, S., D. W. Tank, R. Menon, J. M. Ellermann, S. G. Kim, H. Merkle and K. Ugurbil (1992). "Intrinsic signal changes accompanying sensory stimulation: functional brain mapping with magnetic resonance imaging." Proc Natl Acad Sci U S A **89**(13): 5951-5955.
72. Peng, S. L., J. A. Dumas, D. C. Park, P. Liu, F. M. Filbey, C. J. McAdams, A. E. Pinkham, B. Adinoff, R. Zhang and H. Lu (2014). "Age-related increase of resting metabolic rate in the human brain." NeuroImage **98**: 176-183.
73. Peng, T., R. Niazy, S. J. Payne and R. G. Wise (2013). "The effects of respiratory CO2 fluctuations in the resting-state BOLD signal differ between eyes open and eyes closed." Magn Reson Imaging **31**: 336–345.
74. Pruim, R. H., M. Mennes, D. van Rooij, A. Llera, J. K. Buitelaar and C. F. Beckmann (2015). "ICA-AROMA: A robust ICA-based strategy for removing motion artifacts from fMRI data." Neuroimage **112**: 267-277.
75. Purves, D., G. J. Augustine, D. Fitzpatrick, W. C. Hall, A.-S. LaMantia, J. O. McNamara and S. M. Williams (2001). Neuroscience, Sinauer Associates.
76. Raichle, M. E. and M. A. Mintun (2006). "Brain work and brain imaging." Annu Rev Neurosci **29**: 449-476.
77. Raichle, M. E., A. M. MacLeod, A. Z. Snyder, W. J. Powers, D. A. Gusnard and G. L. Shulman (2001). "A default mode of brain function." Proc Natl Acad Sci U S A **98**(2): 676-682.
78. Reinhard, M., G. Schwarzer, M. Briel, C. Altamura, P. Palazzo, A. King, N. M. Bornstein, N. Petersen, E. Motschall, A. Hetzel, R. S. Marshall, C. J. Klijn, M. Silvestrini, H. S. Markus and F. Vernieri (2014). "Cerebrovascular reactivity predicts stroke in high-grade carotid artery disease." Neurology **83**(16): 1424-1431.

79. Salinet, A. S., T. G. Robinson and R. B. Panerai (2015). "Effects of cerebral ischemia on human neurovascular coupling CO2 reactivity, and dynamic cerebral autoregulation." J Appl Physiol **118**(2): 170-177.
80. Salkind, N. J. (2010). Encyclopedia of Research Design. Thousand Oaks, CA, SAGE publications Inc.
81. Setsompop, K., B. A. Gagoski, J. R. Polimeni, T. Witzel, V. J. Wedeen and L. L. Wald (2012). "Blipped-controlled aliasing in parallel imaging for simultaneous multislice echo planar imaging with reduced g-factor penalty." Magn Reson Med **67**(5): 1210-1224.
82. Shmueli, K., P. van Gelderen, J. A. de Zwart, S. G. Horovitz, M. Fukunaga, J. M. Jansma and J. H. Duyn (2007). "Low-frequency fluctuations in the cardiac rate as a source of variance in the resting-state fMRI BOLD signal." Neuroimage **38**(2): 306-320.
83. Smith, S. M., P. T. Fox, K. L. Miller, D. C. Glahn, P. M. Fox, C. E. Mackay, N. Filippini, K. E. Watkins, R. Toro, A. R. Laird and C. F. Beckmann (2009). "Correspondence of the brain's functional architecture during activation and rest." PNAS Proc Nat Aca Sci USA **106**(31): 13040-13045.
84. Stefanovic, B. and G. B. Pike (2004). "Human whole-blood relaxometry at 1.5 T: Assessment of diffusion and exchange models." Magn Reson Med **52**(4): 716-723.
85. Stefanovic, B., J. M. Warnking, K. M. Rylander and G. B. Pike (2006). "The effect of global cerebral vasodilation on focal activation hemodynamics." Neuroimage **30**(3): 726-734.
86. Strother, S. C., I. Kanno and D. A. Rottenberg (1995). "Commentary and opinion: I. Principal component analysis, variance partitioning, and "functional connectivity"." J Cereb Blood Flow Metab **15**(3): 353-360.
87. Tak, S., J. R. Polimeni, D. J. Wang, L. Yan and J. J. Chen (2015). "Associations of resting-state fMRI functional connectivity with flow-BOLD coupling and regional vasculature." Brain Connect **5**(3): 137-146.
88. Tagliazucchi, E., F. von Wegner, A. Morzelewski, V. Brodbeck and H. Laufs (2012). "Dynamic BOLD functional connectivity in humans and its electrophysiological correlates." Front Hum Neurosci **6**: 339.
89. Tancredi, F. B. and R. D. Hoge (2013). "Comparison of cerebral vascular reactivity measures obtained using breath-holding and CO2 inhalation." J Cereb Blood Flow Metab **33**: 1066-1074.
90. Triantafyllou, C., J. R. Polimeni and L. L. Wald (2011). "Physiological noise and signal-to-noise ratio in fMRI with multi-channel array coils." NeuroImage **55**(2): 597-606.
91. Uludağ, K., B. Müller-Bierl and K. Uğurbil (2009). "An integrative model for neuronal activity-induced signal changes for gradient and spin echo functional imaging." Neuroimage **48**(1): 150-165.
92. Wang, Z., G. K. Aguirre, H. Rao, J. Wang, M. A. Fernández-Seara, A. R. Childress and J. A. Detre (2008). "Empirical optimization of ASL data analysis using an ASL data processing toolbox: ASLtbx." Magn Reson Imaging **26**(2): 261-269.
93. Whitfield-Gabrieli, S. and A. Nieto-Castanon (2012). "Conn: a functional connectivity toolbox for correlated and anticorrelated brain networks." Brain Connect **2**(3): 125-141.
94. Wu, C. W., H. Gu, H. Lu, E. A. Stein, J.-H. Chen and Y. Yang (2009). "Mapping functional connectivity based on synchronized CMRO2 fluctuations during the resting state." NeuroImage **45**(694–701).

95. Xu, G., H. A. Rowley, G. Wu, D. C. Alsop, A. Shankaranarayanan, M. Dowling, B. T. Christian, T. R. Oakes and S. C. Johnson (2010). "Reliability and precision of pseudo-continuous arterial spin labeling perfusion MRI on 3.0 T and comparison with 15O-water PET in elderly subjects at risk for Alzheimer's disease." NMR Biomed **23**(3): 286-293.
96. Yang, H., X.-Y. Long, Y. Yang, H. Yan, C.-Z. Zhu, X. P. Zhou, Y. F. Zang and Q. Y. Gong (2007). "Amplitude of low frequency fluctuation within visual areas revealed by resting-state functional MRI." NeuroImage **36**(1): 144-152.
97. Yeo, B. T., F. M. Krienen, J. Sepulcre, M. R. Sabuncu, D. Lashkari, M. Hollinshead, J. L. Roffman, J. W. Smoller, L. Zöllei, J. R. Polimeni, B. Fischl, H. Liu and R. L. Buckner (2011). "The organization of the human cerebral cortex estimated by intrinsic functional connectivity." J Neurophysiol **106**(3): 1125-1165.
98. Zang, Y. F., Y. He, C. Z. Zhu, Q. J. Cao, M. Q. Sui, M. Liang, L. X. Tian, T. Z. Jiang and Y. F. Wang (2007). "Altered baseline brain activity in children with ADHD revealed by resting-state functional MRI." Brain Dev **29**(2): 83-91.

Appendix

A Supplementary data

Table A.1: Within-subject voxel-wise analysis: functional connectivity vs. CBF_0 in the default-mode network (DMN). DWtest score value > 2 indicates no autocorrelation bias between voxels within each subject. Out of 15 subjects, 8 subjects illustrate positive correlation, 5 subjects illustrate negative correlation, and 2 subjects illustrate no correlation ($p \geq 0.05$).

Subject	DWtest	r	R^2	p
1	2.69	-0.52	0.27	1.11E-04
2	2.13	0.40	0.16	4.44E-03
3	2.11	0.33	0.11	1.96E-02
4	2.39	0.59	0.35	6.83E-06
5	1.98	0.74	0.55	8.95E-10
6	1.79	0.75	0.56	4.87E-10
7	2.52	0.56	0.31	3.02E-05
8	2.30	-0.65	0.42	4.04E-07
9	2.03	0.63	0.39	1.45E-06
10	1.77	-0.46	0.21	1.03E-03
11	2.00	-0.31	0.10	2.92E-02
12	2.93	-0.51	0.26	1.75E-04
13	2.09	-0.28	0.08	5.29E-02
14	2.03	-0.15	0.02	3.00E-01
15	2.15	0.52	0.27	1.47E-04

Table A.2: Within-subject voxel-wise analysis: functional connectivity vs. CBF_0 in the sensori-motor network (SMN). DWtest score value > 2 indicates no autocorrelation bias between voxels within each subject. Out of 15 subjects, 8 subjects illustrate positive correlation, 4 subjects illustrate negative correlation, and 3 subjects illustrate no correlation ($p \geq 0.05$).

Subject	DWtest	r	R^2	p
1	2.67	-0.47	0.22	7.40E-04
2	2.12	-0.49	0.24	4.25E-04
3	2.08	-0.18	0.03	2.19E-01
4	2.14	0.82	0.68	8.14E-13
5	2.41	0.49	0.24	3.46E-04
6	2.24	0.46	0.21	8.97E-04
7	2.27	0.56	0.31	3.05E-05
8	2.53	-0.52	0.28	1.09E-04
9	2.11	0.26	0.07	7.10E-02
10	1.82	0.49	0.24	4.83E-04
11	2.07	0.64	0.41	7.15E-07
12	2.00	-0.48	0.23	5.82E-04
13	2.01	0.87	0.76	1.58E-15
14	1.99	0.09	0.01	5.58E-01
15	2.17	0.70	0.49	2.14E-08

Table A.3: Within-subject voxel-wise analysis: functional connectivity vs. CBF_0 in the visual network (VN). DWtest score value > 2 indicates no autocorrelation bias between voxels within each subject. Out of 15 subjects, 3 subjects illustrate positive correlation, 6 subjects illustrate negative correlation, and 6 subjects illustrate no correlation ($p \geq 0.05$).

Subject	DWtest	r	R^2	p
1	2.05	0.01	0.00	9.29E-01
2	2.30	-0.67	0.45	1.10E-07
3	1.91	0.08	0.01	5.76E-01
4	2.09	-0.11	0.01	4.35E-01
5	2.02	0.46	0.21	1.07E-03
6	2.16	-0.34	0.12	1.59E-02
7	2.35	-0.36	0.13	1.21E-02
8	2.86	0.41	0.17	3.33E-03
9	2.07	0.08	0.01	5.99E-01
10	2.57	-0.29	0.08	4.39E-02
11	2.36	-0.81	0.66	1.95E-12
12	2.07	0.30	0.09	3.50E-02
13	2.06	-0.07	0.00	6.30E-01
14	2.12	-0.21	0.04	1.52E-01
15	2.31	-0.39	0.16	5.11E-03

Table A.4: Within-subject voxel-wise analysis: functional connectivity vs. CVR in the default-mode network (DMN). DWtest score value > 2 indicates no autocorrelation bias between voxels within each subject. Out of 14 subjects, 2 subjects illustrate positive correlation, 6 subjects illustrate negative correlation, and 6 subjects illustrate no correlation ($p \geq 0.05$).

Subject	DWtest	r	R^2	p
1	2.07	-0.67	0.45	1.11E-07
2	2.56	-0.10	0.01	4.90E-01
3	2.24	0.45	0.20	1.22E-03
4	2.32	-0.09	0.01	5.17E-01
5	2.30	-0.32	0.10	2.75E-02
6	2.59	0.26	0.07	7.33E-02
7	2.48	-0.32	0.10	2.64E-02
8	2.01	0.32	0.10	3.46E-02
9	2.56	-0.05	0.00	7.13E-01
10	2.68	-0.32	0.10	2.35E-02
11	2.76	-0.52	0.27	1.37E-04
12	2.25	-0.05	0.00	7.14E-01
13	2.11	-0.18	0.03	2.29E-01
14	2.05	-0.42	0.18	2.97E-03

Table A.5: Within-subject voxel-wise analysis: functional connectivity vs. CVR in the sensori-motor network (SMN). DWtest score value > 2 indicates no autocorrelation bias between voxels within each subject. Out of 14 subjects, 1 subject illustrates positive correlation, 5 subjects illustrate negative correlation, and 8 subjects illustrate no correlation ($p \geq 0.05$).

Subject	DWtest	r	R^2	p
1	2.51	-0.25	0.06	8.79E-02
2	2.01	-0.40	0.16	5.38E-03
3	2.03	-0.13	0.02	3.75E-01
4	2.08	0.40	0.16	5.28E-03
5	2.04	-0.78	0.61	1.66E-10
6	2.24	-0.03	0.00	8.29E-01
7	1.91	-0.33	0.11	2.28E-02
8	1.97	-0.16	0.03	2.93E-01
9	2.19	-0.17	0.03	2.38E-01
10	2.19	-0.58	0.34	1.17E-05
11	2.33	-0.20	0.04	1.74E-01
12	1.99	-0.20	0.04	1.79E-01
13	1.97	0.25	0.06	8.77E-02
14	2.50	-0.31	0.09	3.18E-02

Table A.6: Within-subject voxel-wise analysis: functional connectivity vs. CVR in the visual network (VN). DWtest score value > 2 indicates no autocorrelation bias between voxels within each subject. Out of 14 subjects, 8 subjects illustrate positive correlation, 1 subject illustrates negative correlation, and 5 subjects illustrate no correlation ($p \geq 0.05$).

Subject	DWtest	r	R^2	p
1	2.46	0.10	0.01	5.07E-01
2	2.55	0.90	0.80	2.67E-18
3	2.79	0.52	0.27	1.38E-04
4	2.19	0.88	0.78	5.28E-17
5	2.47	0.69	0.48	4.01E-08
6	2.52	0.95	0.89	1.54E-24
7	2.07	0.59	0.35	8.87E-06
8	2.01	0.98	0.96	1.37E-34
9	2.65	0.20	0.04	1.64E-01
10	2.60	0.04	0.00	7.92E-01
11	1.95	0.94	0.88	2.30E-21
12	2.16	-0.02	0.00	8.94E-01
13	2.21	0.14	0.02	3.49E-01
14	2.06	-0.52	0.27	1.15E-04